Carbohydrate Polymers 310 (2023) 120732

Contents lists available at ScienceDirect

Carbohydrate Polymers

journal homepage: www.elsevier.com/locate/carbpol

Chitin nanofibrils modulate mechanical response in tympanic membrane replacements

Shivesh Anand [a,1], Bahareh Azimi [b,c,1], Mónica Lucena [a], Claudio Ricci [b,d], Mariarita Candito [b,e], Lorenzo Zavagna [b], Laura Astolfi [b,e], Maria-Beatrice Coltelli [b,c], Andrea Lazzeri [b,c], Stefano Berrettini [b,d], Lorenzo Moroni [a], Serena Danti [b,c,2], Carlos Mota [a,*,2]

[a] Department of Complex Tissue Regeneration, MERLN Institute for Technology-Inspired Regenerative Medicine, Maastricht University, Maastricht 6229 ER, the Netherlands
[b] Interuniversity National Consortiums of Materials Science and Technology (INSTM), 50121 Firenze, Italy
[c] Department of Civil and Industrial Engineering, University of Pisa, 56122 Pisa, Italy
[d] Department of Surgical, Medical, Molecular Pathology and Emergency Medicine, University of Pisa, 56126 Pisa, Italy
[e] Bioacoustics Research Laboratory, Department of Neurosciences, University of Padua, 35129 Padua, Italy

ARTICLE INFO

Keywords:
Chitin
Polysaccharide
Nanocomposite
Tissue engineering
Eardrum
Mechanical reinforcement

ABSTRACT

The tympanic membrane (TM), is a thin tissue lying at the intersection of the outer and the middle ear. TM perforations caused by traumas and infections often result in a conductive hearing loss. Tissue engineering has emerged as a promising approach for reconstructing the damaged TM by replicating the native material characteristics. In this regard, chitin nanofibrils (CN), a polysaccharide-derived nanomaterial, is known to exhibit excellent biocompatibility, immunomodulation and antimicrobial activity, thereby imparting essential qualities for an optimal TM regeneration. This work investigates the application of CN as a nanofiller for poly(ethylene oxide terephthalate)/poly(butylene terephthalate) (PEOT/PBT) copolymer to manufacture clinically suitable TM scaffolds using electrospinning and fused deposition modelling. The inclusion of CN within the PEOT/PBT matrix showed a three-fold reduction in the corresponding electrospun fiber diameters and demonstrated a significant improvement in the mechanical properties required for TM repair. Furthermore, *in vitro* biodegradation assay highlighted a favorable influence of CN in accelerating the scaffold degradation over a period of one year. Finally, the oto- and cytocompatibility response of the nanocomposite substrates corroborated their biological relevance for the reconstruction of perforated eardrums.

1. Introduction

The tympanic membrane (TM), also known as the eardrum or the myringa, is a thin tissue lying at the intersection of the outer and the middle ear. Its primary role within the auditory system is to convert sound waves funneled by the outer ear into mechanical motion of ossicular chain in the middle ear (Volandri et al., 2011). TM perforations caused by traumas or microbial infections are the most common injury of the human eardrum. Among them, perforations caused by chronic suppurative otitis media (CSOM), a middle ear inflammatory disease, have been reported to be widespread especially in young children. Global estimates suggest around 31 million new episodes of CSOM every year, with 22 % of them occurring in children below 5 years of age, primarily due to microbial, immunological, and genetically determined factors (Schilder et al., 2016; Verhoeff et al., 2006). The CSOM is accompanied by a persistent discharge through the perforated TM, often resulting in a conductive hearing loss.

Conventional grafting approaches for repairing the damaged TM involve the application of autologous tissues or bioabsorbable materials (Dvorak et al., 1995). However, in the majority of these cases, the lack of consistent material characteristics with respect to the native tissue leads to a suboptimal hearing restoration (Blanshard et al., 1990). The successful sound conduction by the eardrum has been accredited to its unique geometrical and acousto-mechanical properties (Anand et al.,

* Corresponding author.
E-mail address: c.mota@maastrichtuniversity.nl (C. Mota).
[1] These authors contributed equally to this study as first investigators.
[2] These authors contributed equally to this study as senior investigators.

https://doi.org/10.1016/j.carbpol.2023.120732
Received 10 August 2022; Received in revised form 2 February 2023; Accepted 18 February 2023
Available online 23 February 2023

2021; Gan, 2018), whereas other material features such as porosity, timely biodegradation, and immunomodulation are essential for the cellular ingrowth and subsequent wound healing (Danti et al., 2021). Therefore, in recent years, there has been a growing interest in expanding the list of suitable materials for treating the TM perforations. In this regard, tissue engineering has emerged as a promising strategy to propose and develop clinically applicable TM scaffolds (Anand et al., 2022). A wide range of biomaterials including gelatin (Kuo et al., 2018; Lou & He, 2011), silk fibroin (Ghassemifar et al., 2010; Levin et al., 2013), alginate (Weber et al., 2006), poly(ε-caprolactone) (PCL) (Kozin et al., 2016; Lee et al., 2014; Moscato et al., 2020; Seonwoo et al., 2019), and poly(ethylene oxide terephthalate)/poly(butylene terephthalate) (PEOT/PBT) (Anand et al., 2021; Danti et al., 2015; Mota et al., 2015) have been investigated in conjunction with biofabrication techniques, such as fused deposition modelling (FDM) (Anand et al., 2021; Kozin et al., 2016; Mota et al., 2015), bioprinting (Kuo et al., 2018), melt electrowriting (von Witzleben et al., 2021), and electrospinning (ES) (Anand et al., 2021; Danti et al., 2015; Lee et al., 2014; Moscato et al., 2020; Mota et al., 2015; Seonwoo et al., 2019).

Among these, the family of co-poly(ether esters), in particular the PEOT/PBT copolymers has gained notable attention due to their tunable physical and biodegradation properties (Deschamps et al., 2001; Lamme et al., 2008). Several studies have demonstrated the mechanical, acoustical, and biological relevance of PEOT/PBT for TM tissue engineering (Anand et al., 2021; Danti et al., 2015; Grote et al., 1991; Mota et al., 2015). Recently Anand et al. employed PEOT/PBT to examine the role of biomimetic features in eardrum constructs and concluded that the scaffold geometry has a strong impact on the resultant acousto-mechanical response (Anand et al., 2021). The study implemented a dual-scale fabrication approach, combining ES with FDM to manufacture full TM constructs with varying radial and circumferential patterns. In general, the addition of FDM filaments over the electrospun membranes was observed to increase the scaffold stiffness towards that of the native tissue. However, manipulating the scaffold geometry is not always a feasible solution, especially in case of partial TM reconstruction, applied during the repair of medium-size central perforations. In these situations, an adaptable control over the material properties would rather be more advantageous than the highlighted architectural dependency *per se*.

Various strategies have been investigated for modulating the inherent polymer behavior within the manufactured scaffolds. In this respect, CN have been used as a favorable nanofiller agent for reinforcing both natural and synthetic polymeric matrices (Chen et al., 2019; Shankar et al., 2015). Derived from chitin, one of the most abundant polysaccharide in nature (Elieh-Ali-Komi & Hamblin, 2016), CN are known to exhibit excellent biocompatibility, biodegradation, immunomodulation and antimicrobial activity (Danti et al., 2021), while enhancing the resultant mechanical characteristics of the polymer matrix. Moreover, they are extracted from food biowaste, such as chitin-rich shells of shrimps, crabs, or krill, which makes them an affordable, readily available, and renewable biomaterial. The application of CN for tissue engineering has commonly been investigated in the form of nanocomposites in combination with thermoplastics, such as PCL (Ji et al., 2012), poly(lactic acid) (Coltelli et al., 2019), and poly(ethylene oxide) (Kuo & Ku, 2008). In all these studies, the successful dispersion of CN within the nanocomposites has been noted crucial for their effectiveness as a reinforcement agent. Several approaches have been explored in this regard. Among them, the use of poly(ethylene glycol) (PEG) as a compatibilizing agent has specifically been advantageous in reducing interfacial tension and promoting homogeneity within nanocomposite matrices (Brown & Laborie, 2007; Li et al., 2017). The combination of CN with PEG has been reported to demonstrate significant improvements in the mechanical, antimicrobial, and anti-inflammatory properties of the produced composites, as compared to their pristine counterparts (Coltelli et al., 2019; Kuo & Ku, 2008; Li et al., 2017).

The primary goal of this work was to study the relevance of CN in creating mechanically suitable replacements for treating TM perforations. It is hypothesized that the introduction of CN within polymeric scaffolds can favorably reinforce the material properties required for reconstructing the damaged TM. Considering the current gap highlighted in modulating the mechanical behavior of a scaffold without manipulating its polymer composition or geometry (Anand et al., 2021), the application of such carbohydrate-based nanocomposites offers a novel approach for TM regeneration. Distinct CN/PEG ratios were chosen and evaluated to achieve an optimal dispersion of CN within the polymeric matrix. The resultant PEOT/PBT/(CN/PEG) nanocomposites were tested to create biomimetic replacements for both partial and total reconstruction of the perforated eardrum. In this regard, the composite processability was assessed for two key biofabrication technologies, ES and FDM, with respect to previously reported efforts in this direction (Anand et al., 2021; Mota et al., 2015). Subsequently, the influence of CN was investigated on the surface morphology, mechanical properties, *in vitro* biodegradation, and cytocompatibility of the fabricated scaffolds. Additionally, TM-specific indentation measurements were conducted to corroborate their functional response for eardrum tissue engineering. By highlighting the structural reinforcement offered by CN, this work aims to demonstrate the potential of CN-based therapies for reconstructing the impaired TM with the required material characteristics for an effective sound transmission (Fig. 1).

2. Materials and methods

2.1. Materials

An aqueous suspension of 2 % (w/w) CN was supplied by Texol s.r.l. (Italy). The CN, cosmetic grade, were produced by treating crustacean-derived chitin with hydrochloric acid under boiling conditions (Muzzarelli & Morganti, 2013). After a series of successive centrifugation and decantation, the obtained nanofibrillar chitin was resuspended in sterile distilled water. The final colloidal suspension has a pH of 5, and a deacetylation degree of around 10 % (Muzzarelli & Morganti, 2013). The average length of the resultant CN was 20 μm, whereas the average width was 90 nm (Coltelli et al., 2019).

PEOT/PBT was kindly provided by PolyVation B.V. (the Netherlands). The 300PEOT55PBT45 grade of the copolymer was selected for this study based on previous literature (Anand et al., 2021; Danti et al., 2015; Mota et al., 2015). The aPEOTbPBTc notation indicates the polymer composition, where "a" represents the molecular weight (M_w = 300 g/mol) of starting PEG blocks, and "b/c" (55/45) denotes the weight ratio of PEOT/PBT, respectively. For the current lot of the copolymer (PA-01/17-01), the average M_w of 93 kDa was quantified by gel permeation chromatography, and the glass transition temperature (T_g) of −22 °C and the melting temperature of 154 °C was measured using differential scanning calorimetry.

PEG with a number average molecular weight (M_n) of 4000 g/mol (code: 81240) was supplied by Sigma Aldrich (Italy) in the form of platelets, chloroform of 99.5 % purity by Merck KGaA (Germany), and hexafluoro-2-propanol (HFIP) of analytical grade by Biosolve B.V. (the Netherlands). Absolute ethanol (EtOH; 99.8 % purity), phosphate buffered saline (PBS), Low-Glucose DMEM, L-glutamine, Fluconazole, Penicillin and Streptomycin (pen-strep), gelatin (type B, from bovine skin), 4,6-diamideino-2-phenylindole dihydrochloride (DAPI), and propidium iodide were supplied by Sigma-Aldrich *via* Merck KGaA (Germany), sterile saline solution by Fresenius Kabi (Germany), formalin by Bio-Optica (Italy), Horse Serum (HS) by CARLO ERBA Reagents (Italy), and heat-inactivated fetal bovine serum (FBS) by Invitrogen *via* Thermo Fisher Scientific (USA). For the culture of Organ of Corti cells, the mouse cell line OC-k3 was obtained from House Ear Institute (USA). Dulbecco's Modified Eagle Medium (DMEM), RPMI medium were supplied by Gibco BRL (USA). Interferon γ (IFN) was obtained from Genzyme (USA), and CellTiter 96® AQueous MTS

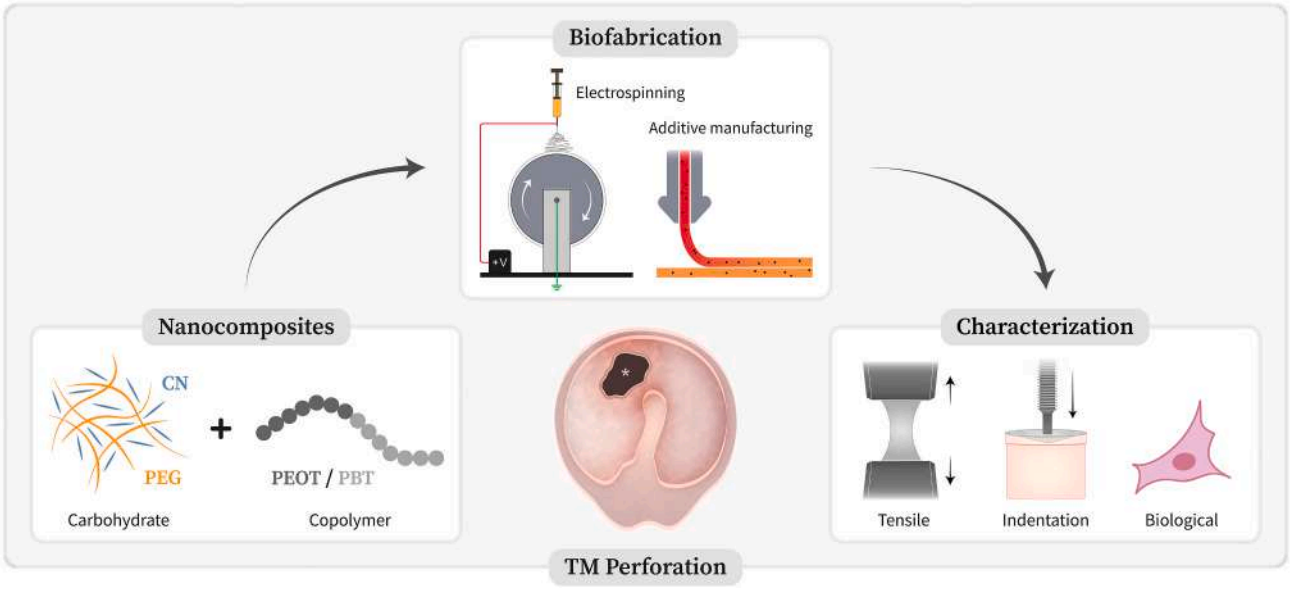

Fig. 1. Schematic diagram illustrating the overall flowchart of the study presented herein. The asterisk (*) highlights a medium-size central perforation of the tympanic membrane (TM).

Reagent Powder from Promega Corporation (USA). Human mesenchymal stromal cells (hMSCs) were supplied by Merck Millipore S.A.S. (USA). AlamarBlue®, Alexa Fluor™ 488 phalloidin, and α-minimal essential medium with Glutamax (α-MEM) was bought from Thermo Fisher Scientific (USA).

2.2. Nanocomposite preparation

Melt blending was implemented for nanocomposite preparation to minimize the use of organic solvents. PEG was employed as the compatibilizing agent to achieve a homogenous distribution of CN within the PEOT/PBT/(CN/PEG) composites. Different CN/PEG weight ratios, namely 50:50, 65:35, 70:30, and 75:25 (% w/w), were investigated. The precursor dispersions were prepared by adding the corresponding amounts of PEG to CN solution under constant stirring for 2 h at room temperature (RT). The resultant solutions were then transferred to petri dishes and dried under a ventilated fume hood until solidification.

The solidified CN/PEG pre-composites were pulverized into fine powder using mortar and pestle until a homogeneous powder was obtained. This powder along with PEOT/PBT pellets was fed into a Thermo Haake Minilab II twin screw extruder (Germany) through the hopper placed at the beginning of the twin screws. All the components were mixed thoroughly in the recirculating channel of the extruder. Finally, the extrusion was carried out at 165 °C and 100 revolutions per minute (rpm) for 1 min to obtain the melt blended PEOT/PBT/(CN/PEG) nanocomposites with varying CN/PEG ratios. A consistent concentration of 2 % (w/w, with respect to PEOT/PBT) CN was maintained across all the conditions.

2.3. Film preparation

Films were produced for a preliminary characterization of all the nanocomposite formulations. Compression molding was used where bulk PEOT/PBT/(CN/PEG) nanocomposites were subjected to a manual press (Lab Press 10 T, Noselab ATS, Italy) at 170 °C for 2 min.

2.4. Material characterization

2.4.1. Cyto- and otocompatibility of pristine CN

Cytocompatibility of pristine CN were assessed using hMSCs cultured in α-MEM supplemented with 10 % FBS, 1 % PS and with varying concentrations of CN: 0 μg/mL, 10 μg/mL, 100 μg/mL and 1000 μg/mL for 7 days under standard conditions (37 °C, 5 % CO_2). PrestoBlue™ assay was performed at day 1, 3 and 7 to quantify the cell metabolic activity. At day 1 and 7, samples were fixed with 3.7 % paraformaldehyde and stained with Alexa Fluor™ 488 phalloidin and DAPI to visualize the F-actin filaments and the nuclei, respectively. Finally, fluorescence images were acquired on an inverted microscope (Nikon Eclipse Ti-E, the Netherlands).

Otocompatibility was assessed using inner ear representative cell lines, such as OC-k3 (organ of Corti), HaCaT (epidermal keratinocytes) and PC12 (neural-like cells). The PC12 cells were grown in 5 % CO_2 at 37 °C in RPMI medium supplemented with 10 % HS, 5 % FBS, 2 mM L-Glutamine, 1 % pen-strep. HaCaT cells were grown in 5 % CO_2 at 37 °C in DMEM, supplemented with 10 % FBS, 2 mM L-Glutamine, 1 % pen-strep. OC-k3 cells were grown in 10 % CO_2 at 33 °C in DMEM High Glucose medium supplemented with 10 % FBS, 1 % pen-strep, 2 mM L-glutamine, and 50 U/mL of IFN. The following day the 3 cell types were treated with three different concentrations of CNs: 20 μg/mL, 10 μg/mL and 5 μg/mL diluted in complete medium. The cell viability on the three cell lines was analyzed by a cytofluorimeter (FACSCalibur, BD Biosciences, USA). The percentage of cells dead, stained by propidium iodide (PI, 50 μg/mL, Sigma Aldrich, Milan, Italy) was measured using a standard optical filter 585/42 nm (FL2). The experiments were performed two times ($n = 2$) with 3 replicates for each treatment.

2.4.2. X-ray diffraction

The crystallinity of the materials was assessed through X-ray diffraction (XRD; Bruker D2 Phaser, the Netherlands). X-ray diffractograms were collected using Cu Kα radiation ($\lambda = 1.5406$ Å) between $5° \leq 2\theta \leq 70°$ in increments of 0.02°.

2.4.3. Fourier-transform infrared spectroscopy

The chemical composition of the fabricated films was analyzed using Fourier transform infrared spectrometer (FTIR; Nicolet 380, Thermo Scientific, USA) equipped with a Smart™ iTX accessory comprising a monolithic diamond attenuated total reflection (ATR) crystal. FTIR spectra were recorded in the 4000–500 cm^{-1} range at 2 cm^{-1} spectral resolution and 128 scans per sample. Background spectra were collected before each sample to eliminate signals of the spectrometer and its

environment from the sample spectrum.

2.4.4. Dynamic light scattering

The conductivity and zeta potential of CN and CN/PEG colloidal suspensions were measured with dynamic light scattering (DLS; Zetasizer Nano, Malvern Panalytical, UK). Solidified crystals of CN and CN/PEG were suspended in Milli-Q water by ultrasonication at 37 °C for 5 min. An initial colloidal concentration of 5000 μg/mL was prepared for both the materials, which was serially diluted to obtain the subsequent concentrations of 1000 μg/mL, 100 μg/mL, 10 μg/mL, and 1 μg/mL.

2.4.5. Thermogravimetric analysis

Thermal stability of the prepared nanocomposite was evaluated using thermogravimetric analysis (TGA; Q500, TA Instruments, United States). A linear increase in temperature from 25 °C to 500 °C at the rate of 10 °C/min was applied in a nitrogen atmosphere.

2.4.6. Field emission scanning electron microscopy

Morphological characterization of the nanocomposite films and bulk filaments was performed using field emission scanning electron microscopy (FE-SEM; Quanta™ 450 FEG, Field Electron and Ion Company, USA). The cross-sectional surface of the compounded filaments was obtained by cryofracture for each CN/PEG ratio. Samples were sputtered with platinum (EM ACE600, Leica Microsystems, Germany) and imaged at an accelerating voltage of 10 kV and working distance of 10 mm. The thickness of the films was measured using a portable thickness gauge (model 2050F, Mitutoyo Europe GmbH, Germany).

2.5. Computational modelling

A previously reported Python toolkit was utilized to generate a biomimetic geometry for the full reconstruction of the TM (Anand et al., 2021). Specific parameters were chosen to obtain a computer-aided design (CAD) with the optimal shape, dimension, and fiber density of the radial and circumferential filaments. The exterior proportions were set based on the anatomical dimensions of the human TM (Anand et al., 2022): 8.5 mm for the horizontal diameter, 9.5 mm for the slightly longer vertical diameter, and 100 μm for the thickness. Subsequently, computational models (COMSOL Multiphysics 6.0, Comsol B.V., the Netherlands) were designed to simulate the mechano-acoustical response of the resultant geometry in comparison to the native tissue. This was achieved by implementing the *structural mechanics* and *acoustics* modules of COMSOL as described in an earlier publication (Anand et al., 2021). Moreover, the material properties of human eardrum, in particular, the density, Young's modulus (E), and Poisson's ratio of *pars tensa*, were obtained from the literature (Caminos et al., 2018).

All theoretical computations were performed within the linear elastic regime. Finally, the selected geometry was validated with respect to the E value (mechanical) and resonant frequencies (acoustical) computed for the respective TM models – reconstructed (R) and native (N).

2.6. ES of nanocomposites

ES was applied to manufacture PEOT/PBT/(CN/PEG) TM scaffolds. Two approaches were investigated for the preparation of the ES solutions. The first approach, the melt blended nanocomposite was dissolved in a 70:30 (v/v) solvent mixture of chloroform and HFIP, by stirring overnight at ambient conditions. For the second approach, an equivalent CN/PEG powder was added to a PEOT/PBT previously dissolved in a 70:30 (v/v) solvent mixture of chloroform and HFIP and stirred overnight at ambient conditions. A concentration of 18 % (w/v) was used for preparing these precursor ES solutions. The ES was performed on Fluidnatek LE-100 (Bioinicia S.L., Spain) in a controlled environment, set at 23 °C and 40 % of relative humidity.

Previously reported operating parameters were adapted to fabricate homogeneous nanofibrous meshes containing CN (Anand et al., 2021; Danti et al., 2021). A voltage of 20 kV was applied to collect the electrospun fibers on a cylindrical mandrel (stainless steel, diameter = 200 mm, length = 300 mm). The collector was wrapped with aluminum foil assembled with circular bands (inner diameter = 12 mm, outer diameter = 15 mm) of Finishmat 6691 LL (Lantor B.V., the Netherlands). The supporting band allowed an easy handling of the thin membranes, especially after removal of the aluminum foil substrate for the subsequent morphological, mechanical, and biological characterizations. The PEOT/PBT/(CN/PEG) precursor solution was ejected through a 0.8 mm spinneret at a flow rate of 0.9 mL·h^{-1}. A consistent air gap of 10 cm was maintained. The collector rotation was set at 150 rpm, and the ES was conducted for 60 min to manufacture the final TM scaffolds. However, a longer ES duration of 90 min was used for producing thicker meshes employed for the degradation studies. Following the fabrication, all electrospun meshes were left overnight inside a fume hood to evaporate any residual traces of the organic solvents.

SEM (Jeol JSM-IT200, the Netherlands) was performed to examine the nanofibrous morphology of the electrospun meshes. Samples were coated with a thin layer of gold (Quorum Technologies SC7620, UK) prior to the imaging. SEM micrographs were captured at an accelerating voltage of 10 kV and working distance of 10 mm. The subsequent post-processing and image analysis was carried out on Fiji software (https://fiji.sc/), where the average fiber diameter was calculated for each condition (n = 150).

2.7. FDM of nanocomposites

FDM was performed to evaluate the manufacturing of PEOT/PBT/(CN/PEG) nanocomposites scaffolds for the full reconstruction of the human eardrum. G-code for the computationally validated TM geometry was generated using the Python toolkit (Anand et al., 2021), and loaded on a FDM based additive manufacturing system (BioScaffolder, SYSENG, Germany). The material deposition was initiated by melting the polymer at 190 °C, following which it was extruded using a combination of mechanical screw-driven and pneumatic pressure. The screw rotational speed was set at 70 rpm and the pressure at 750 kPa. The translational velocity was maintained constant at 157 mm·min^{-1}. Four different nozzles were tested for the fabrication process – (1) stainless steel with ID of 260 μm (ID260, BL25E02A, DL technologies, USA), (2) stainless steel with ID of 184 μm (ID184, BL28E03A, DL technologies, USA), (3) stainless steel with ceramic tip and ID of 100 μm (ID100, DL32005AC, DL technologies, USA), and (4) stainless steel with ceramic tip and ID of 70 μm (ID70, DL003005AC, DL technologies, USA).

Dual-scale PEOT/PBT/(CN/PEG) nanocomposite-based TM scaffolds were manufactured as a proof-of-concept by depositing the FDM filaments on prefabricated electrospun meshes.

2.8. Mechanical characterization

The mechanical response of the chosen compositions was evaluated independently for the preliminary films and for the TM-specific scaffolds. Tensile measurements were performed to compare the different nanocomposite formulations, followed by a functionally relevant characterization for the TM (*i.e.*, macroindentation) on select conditions.

Tensile properties of the films were characterized by INSTRON 5500R mechanical tester equipped with MERLIN software (USA). A 100 N load cell was used for this at a scan rate of 100 mm·min^{-1}. The film samples were prepared with a width of 4 mm and length of 27 mm.

Mechanical measurements on the electrospun scaffolds were carried out on TA ElectroForce 3200 mechanical tester (USA). Samples were cut in rectangular strips, and the tests were performed at RT until failure. The length and width of each sample was measured with a digital caliper, and the thickness was calculated from SEM cross-sections. A 45 N load cell was used with a scan rate of 0.003 mm·s^{-1} until failure. In addition, macroindentation was conducted for the pristine PEOT/PBT and PEOT/PBT/(CN/PEG) nanocomposite with 50:50 CN/PEG ratio. A

previously reported a custom setup was implemented to indent circular scaffolds at a scan rate of 0.003 mm·s^{-1} (Anand et al., 2021).

2.9. Biodegradation characterization

The biodegradation behavior of the electrospun fibrous meshes was investigated by monitoring the weight changes of 3 × 3 cm^2 samples, in triplicates. Scaffolds with a higher thickness (400 ± 5 μm), were employed to obtain more precise weight measurements. The 50:50 ratio of CN/PEG was chosen as the representative condition for the PEOT/PBT/(CN/PEG) composites, which was compared to their pristine PEOT/PBT counterpart. Samples were prepared by washing the electrospun meshes in 10 mL distilled water for 20 min, followed by dehydration in 5 mL absolute EtOH for 3 min, and finally, evaporation under a ventilated hood for 3 h. The rate of degradation was studied by immersing the samples in 10 mL sterile saline solution (0.9 % NaCl) placed in a 37 °C oven. Weight changes were monitored over a period of one year using an analytical balance (AS 220.R2, RADWAG, Poland). The samples were weighed, and the saline solution was refreshed every week during the first five months; after which the weights were recorded once a month and the solution was changed every two weeks. To avoid errors in terms of the liquid trapped within the electrospun meshes, all measurements were normalized with respect to their corresponding sample weights recorded at the start of the study.

At the end of 12 months, SEM analysis was conducted to inspect the surface and cross-sectional morphology of the biodegraded samples.

2.10. Biological characterization of nanocomposite substrates

Direct and indirect *in vitro* cytocompatibility tests were performed to evaluate the interaction of the nanocomposites with relevant cell types for TM applications. All the samples were sterilized with absolute EtOH overnight, followed by three rinses in fluconazole and pen-strep supplemented PBS for 10 min. Subsequently, the materials were placed in a 24-well plate and treated with sterile filtered 2 % (w/v) gelatin aqueous solution for 30 min.

2.10.1. Otocompatibility evaluation

An organ of Corti cell line, OC-k3, was used to determine any ototoxic effects of the PEOT/PBT/(CN/PEG) nanocomposites. A total of 150,000 cells/well were seeded and maintained at 33 °C, 10 % CO_2 in DMEM supplemented with 10 % FBS, 50 U/mL of IFN and 1 % pen-strep. For direct ototoxicity test, the OC-k3 cells were cultured on pre-treated nanocomposite films. On the other hand, for indirect cytocompatibility tests, the films were incubated in the culture medium for 24 h, following which, the conditioned culture media was administrated to pre-cultured OC-k3 cells on tissue culture plate. Two time-points, 24 h and 48 h, were chosen to assess the subsequent cell viability in both the cases, as they are predictive of oto-toxicity (Bertolaso et al., 2001). This was quantified using CellTiter 96® Aqueous Non-Radioactive Cell Proliferation Assay based on the manufacturer's protocol.

2.10.2. Cytocompatibility evaluation

HMSCs have been employed extensively for the TM regeneration (Maharajan et al., 2020). Therefore, considering their growing relevance in eardrum tissue engineering, the influence of PEOT/PBT/(CN/PEG) composites was investigated on the attachment and viability of hMSCs. Preliminary films were used for this, along with the 50:50 electrospun scaffold. A cell density corresponding to 150,000 cells per well was seeded onto the samples and maintained in culture for 8 days under standard conditions (37 °C, 5 % CO_2). The cell viability was monitored with respect to their metabolic activities on day 1, 4, and 8. AlamarBlue® test was conducted in this regard, where the dye reduction percentage (%AB_{red}) was calculated following the absorbance double reading method (Eq. (A.1): Appendix A).

At the end of 8 days, the cultured constructs were imaged under SEM to analyze the eventual cell distribution. Samples were prepared by fixing them in 1 % (w/v) neutral buffered formalin for 10 min at 4 °C, followed by dehydration in 70 % (v/v) EtOH for 30 min, and finally, overnight drying in vacuum oven at 37 °C.

2.11. Statistical analysis

All samples were assigned randomly to the different experimental groups. Wherever applicable, the data has been expressed as mean ± standard deviation. The number of replicates (n) is specified in the figure captions along with the statistical test performed. The statistical tests were performed with GraphPad Prism 8 (GraphPad Software, USA), where the statistical significances were determined by applying a one-way or two-way analysis of variance (ANOVA) followed by a Student's t-test or Tukey's honestly significant difference (HSD) post-hoc test (*$p < 0.05$, **$p < 0.01$, ***$p < 0.005$, ****$p < 0.0001$ and not significant (*n. s.*) for $p > 0.05$).

3. Results

3.1. Chitin and nanocomposite film characterization

Material characterization and biological characterizations were performed to the chitin and the resultant nanocomposites films. HMSCs exposure to different pristine CN concentrations showed no noticeable change in cell morphology (Fig. 2A) and a qualitative assessment revealed an identical increase of the metabolic activity over the culture period of 7 days (Fig. 2B). Furthermore, the CN were tested using an inner cell model, which includes three different cell lines: OC-k3 cells as a model of sensory epithelium, HaCaT cells as a model of normal epithelial, and PC12 cells as a model of neural cells. In all these cell lines viability was not affected by the administration of CN up to 20 μg/mL concentration in 48 h (Fig. S1).

DLS measurements were performed to investigate the protonation ability of deacetylated amine groups in the current CN (Fig. 2C–D). Homogeneous colloidal suspensions of CN and CN/PEG in Milli-Q water (inset, Fig. 2C) showed a gradual increase in the conductivity with the increase of chitin concentration (Fig. 2C). However, no such trend was noted in case of the zeta potential (Fig. 2D). The suspensions demonstrated a significant elevation with the addition of CN, but the subsequent increase in colloidal concentrations did not affect the zeta potential values.

XRD analysis was conducted to validate the incorporation of CN in the PEOT/PBT/(CN/PEG) nanocomposite (Fig. 2E). Characteristic peaks of CN crystallinity at 9.4°, 19.4° and 23.6° were detected in its subsequent combinations with PEG and PEOT/PBT. TGA measurements were conducted to verify the thermal stability of the resultant nanocomposites with respect to the pristine PEOT/PBT (Fig. 2F). An identical curve was obtained for both the polymers, which confirmed that PEOT/PBT/(CN/PEG) remained stable until 300 °C.

FTIR-ATR performed on the nanocomposite films and their pristine counterparts validated the presence of CN (Figs. S2–3). Different ratios of CN/PEG pre-composites were analyzed and compared with PEG granule and CN powder (Fig. S2A). Characteristic bands for CN were observed at 1010 cm^{-1} and 1070 cm^{-1}, typically denoting the presence of C—O stretching, 1552 cm^{-1} of secondary amide, 1619 cm^{-1} and 1656 cm^{-1} of primary amide, 2874 cm^{-1} of C—H stretching, 3102 cm^{-1} and 3256 cm^{-1} of N—H stretching in the amide and amine groups, and finally, 3439 cm^{-1} of O—H stretching (Brugnerotto et al., 2001). In the spectrum of pristine PEG, the absorption band at 1633 cm^{-1} can be attributed to a C═C aliphatic double bond, and the peak at the wavelength of 1724 cm^{-1} corresponds to the C═O stretching (Askari et al., 2019). All these bands were noted in case of the CN/PEG pre-composites as well.

To assess the successful dispersion of CN within the polymeric matrix, morphological characterization of the produced nanocomposites

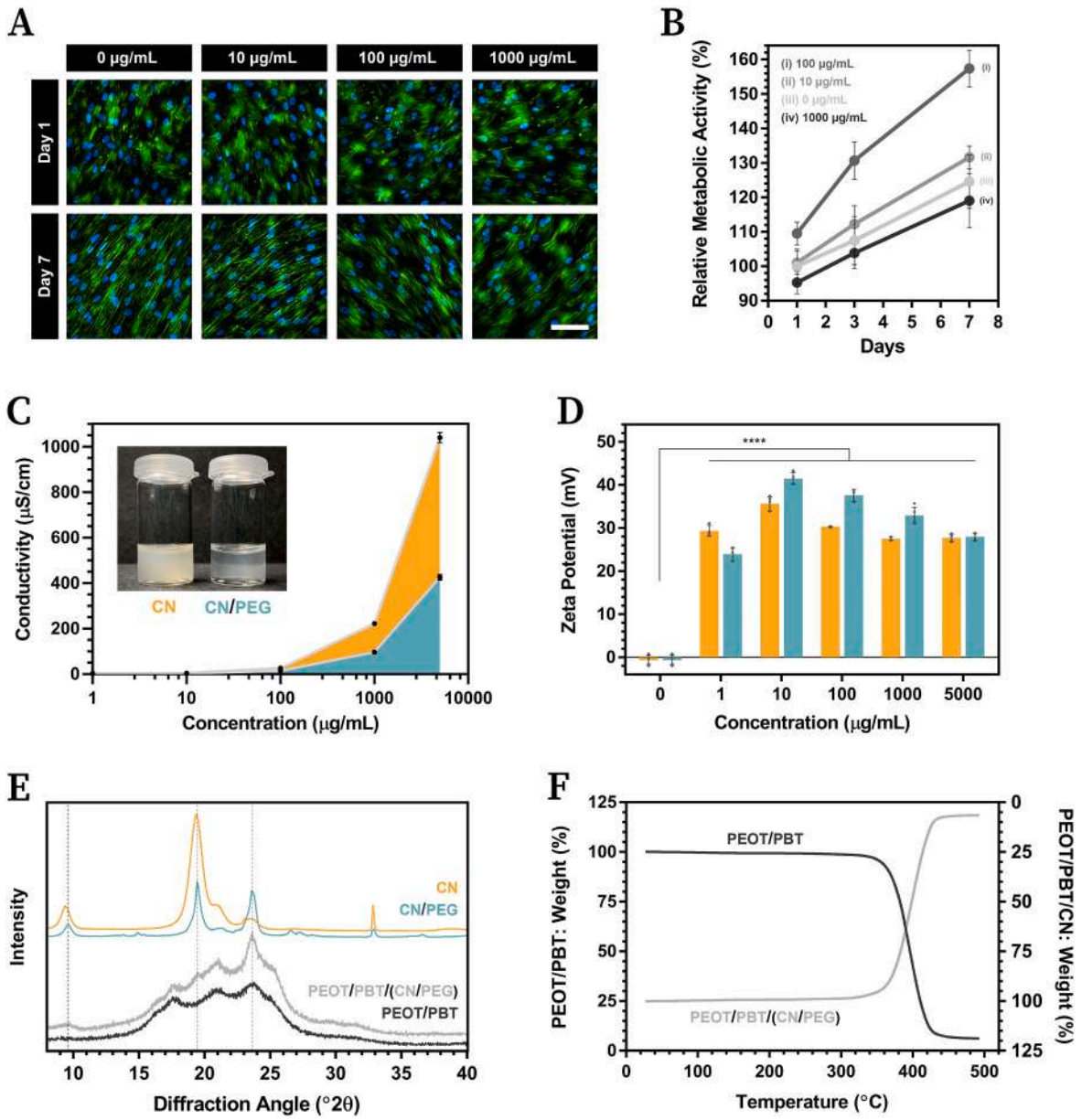

Fig. 2. Carbohydrate and nanocomposite characterization. (A, B) HMSCs cytocompatibility to CN: (A) Phalloidin labeled F-actin (green) and DAPI nuclear staining (blue) at days 1 and 7 for cells cultured with increasing CN concentration. Scale bar: 100 μm; (B) Cell metabolic activity at days 1, 3 and 7 quantified with PrestoBlue™ assay. (C, D) DLS measurements demonstrating the increase in ionic charges with the addition of CN and CN/PEG through (C) conductivity and (D) zeta potential quantifications. (E) XRD spectrum of 50:50 composition of PEOT/PBT/(CN/PEG) compared with that of pristine CN, CN/PEG and PEOT/PBT. (F) TGA analysis of pristine PEOT/PBT and the 50:50 composition of PEOT/PBT/(CN/PEG). (For interpretation of the references to colour in this figure legend, the reader is referred to the web version of this article.)

was conducted. Cross-section of bulk filaments (Fig. S2B) and planar surface of the films (Fig. S3B) analyzed by FE-SEM of the cryo-fractured filaments revealed a homogeneous distribution of the pre-composite inside the PEOT/PBT matrix compounded with a CN/PEG ratio of 50:50 (Fig. S2B (i)). On the contrary, nanocomposite formulations containing a lower PEG content (35 %, 30 %, and 25 %) demonstrated the presence of large pre-composite aggregates, marked by appearance of cracks within their cross-sectional surfaces (Fig. S2B (ii)–(iv)).

The characterization of PEOT/PBT/(CN/PEG) nanocomposites, in terms of their chemical composition and CN dispersion, was conducted on films as they are simple, reproducible and frequently used to analyze material compositions used in tissue engineering (Cima et al., 1991).

Fig. S3B shows FTIR spectra of pristine PEOT/PBT, pristine CN, pristine PEG, and compression molded PEOT/PBT/(CN/PEG) films. Careful inspection of the obtained results confirmed the presence of CN within all the nanocomposite formulations. However, no noticeable differences were detected between the chosen CN/PEG ratios.

In addition, morphological characterization of the films was performed to evaluate the dispersion of CN on planar surfaces (Fig. S3B). The corresponding FE-SEM results were in accordance with the copolymer/pre-composite interactions observed in the bulk filaments. In general, a higher PEG content led to a superior pre-composite dispersal with only sub-micrometric scale irregularities spotted on the film surface (Fig. S3B (i)). On the other hand, evident surface defects distinguished by increased roughness and porosity, were detected within formulations containing a PEG concentration lower than 50 % (w/w), thereby indicating formation of aggregates (Fig. S3B (ii)–(iv)). Finally, the cross-sectional morphology of the films, exhibited a thickness

measurement of 200 ± 2 μm.

3.2. TM scaffold design and modelling

The effective sound conduction by a healthy eardrum is facilitated by its unique 3D architecture comprising radially and circumferentially distributed collagen fibers. Therefore, previously reported computational models were implemented to identify the requisite scaffold geometry for a full TM reconstruction. A biomimetic design consisting of 24 radial filaments and 1 circumferential filament was selected in this regard (Fig. 3A). *In silico* simulations performed on this reconstructed TM (*R*) confirmed a comparable mechano-acoustical response with respect to the native tissue (*N*). The macroindentation-based COMSOL model demonstrated an *E* value of 37 MPa for the chosen TM scaffold in contrast to 32 MPa for the human eardrum (Fig. 3B). Furthermore, the eigenfrequency analysis validated an identical acoustic-structure interaction by displaying similar modes of vibrations occurring at matching resonant frequencies (Fig. 3C).

3.3. ES of nanocomposites

PEOT/PBT has been frequently explored to create electrospun scaffolds for tissue engineering applications (Gonçalves de Pinho et al., 2019; Günday et al., 2020; Malheiro et al., 2021; Zonderland et al., 2020). However, the current study aimed at investigating the influence of the addition of CN to this copolymer matrix (Fig. S4A). SEM images of the fabricated electrospun meshes indicated a significant decrease in the fiber diameters upon the inclusion of CN (Fig. 4A). Almost a three-fold reduction was noted for all the CN/PEG ratios with respect to an average diameter of 1135 ± 168 nm obtained for pristine PEOT/PBT scaffolds (Fig. 4B). Moreover, the frequency distribution analysis showed production of more uniform fibers with PEOT/PBT/(CN/PEG) in comparison to the copolymer alone (Fig. 4C–G). No clear differences were observed between the chosen CN/PEG compositions, and they were all noted to be equally favorable for ES. In addition, the two ES solution preparation approaches (melt and solution) investigated for producing the PEOT/PBT/(CN/PEG) electrospun meshes yielded comparable results (Fig. S5), thereby confirming their appropriateness for the process.

3.4. FDM of nanocomposites

To further evaluate the biofabrication capabilities of PEOT/PBT/(CN/PEG) nanocomposites for TM reconstruction, an FDM-based additive manufacturing technique was investigated. The pre-selected TM pattern was applied and a parametric optimization for the four nozzles with varying internal diameters was performed. Among the chosen needles, ID260 and ID184 demonstrated excellent printability and yielded an average filament diameter of 496 ± 9 μm and 192 ± 18 μm for the nanocomposites tested (Fig. 5A). Moreover, the obtained diameters were found to be comparable to that for the pristine PEOT/PBT (Table 1). Smaller nozzle sizes, namely ID100 and ID70, failed to maintain a consistent flow of the molten nanocomposites and unsuitable for printing.

Within the successfully fabricated scaffolds, agglomerations of CN in the form of brown spots were detected across all the nanocomposite formulations. Fig. 5B presents a schematic depiction of this phenomenon during the melt-extrusion of PEOT/PBT/(CN/PEG). Furthermore, the presence of these spots was also confirmed using SEM (Fig. 5C). These CN aggregates were hypothesized to be the major cause behind the frequent clogging of ID100 and ID70 needles during printing (Fig. S4B).

Finally, dual-scale TM constructs were manufactured as a proof of concept using 50:50 CN/PEG condition of PEOT/PBT/(CN/PEG) nanocomposites (Fig. 5D–E) with the ID184 needle. The hybrid fabrication strategy was realized by depositing FDM filaments on top of electrospun meshes also created with the 50:50 composite. Due to the limited manufacturability of the dual-scale TM scaffolds with an overall thickness below 100 μm, only ES meshes were used for the remaining studies.

3.5. Mechanical characterization

Preliminary mechanical response of the PEOT/PBT/(CN/PEG)

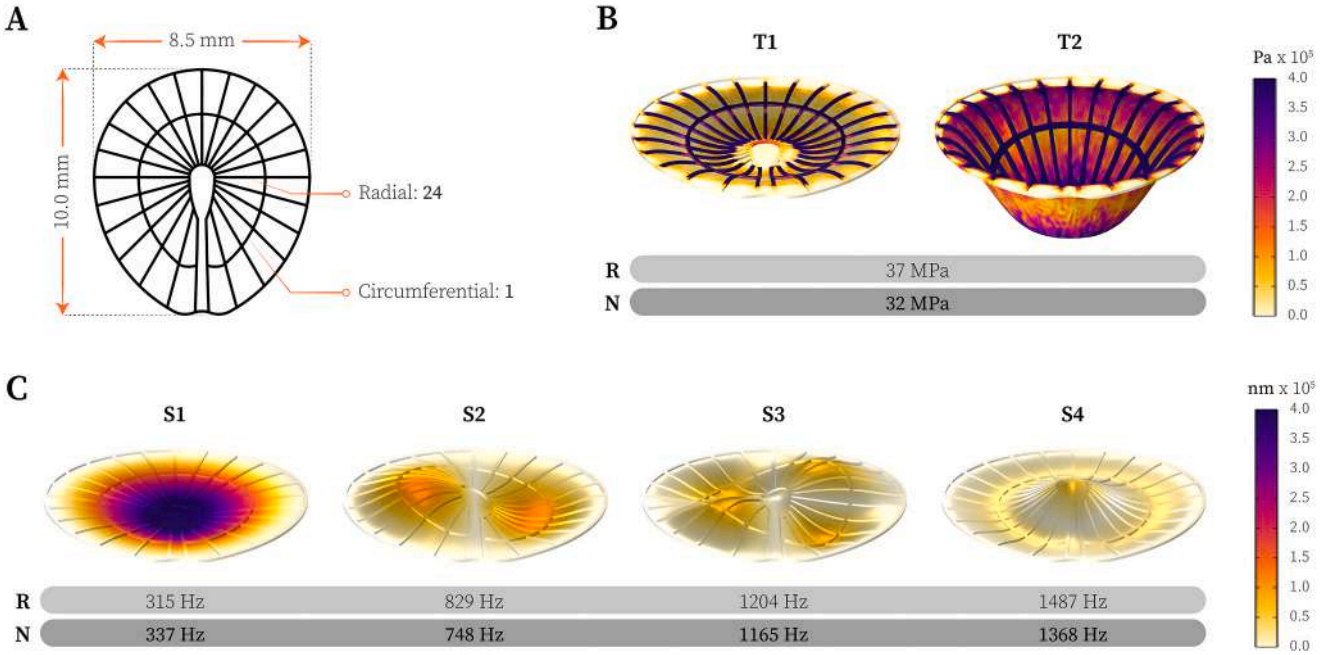

Fig. 3. Scaffold design and modelling. (A) Biomimetic geometry chosen for the full reconstruction of human tympanic membrane (TM). (B, C) Theoretical models on COMSOL Multiphysics predicting the mechano-acoustical response of the chosen scaffold geometry. (B) Indentation-based mechanical measurement simulated at a scan-rate of 3 μm·s^{-1}: (T1) 250 s and (T2) 1000 s. A comparable Young's modulus was calculated for the reconstructed TM (*R*) with respect to the native tissue (*N*). (C) Eigenfrequency-based analysis demonstrating the different modes of vibrations (S1–S4) generated at a constant sound pressure of 0.02 Pa. Analogous to the mechanical response, similar resonant frequencies were noted for the reconstructed (*R*) and native (*N*) TM.

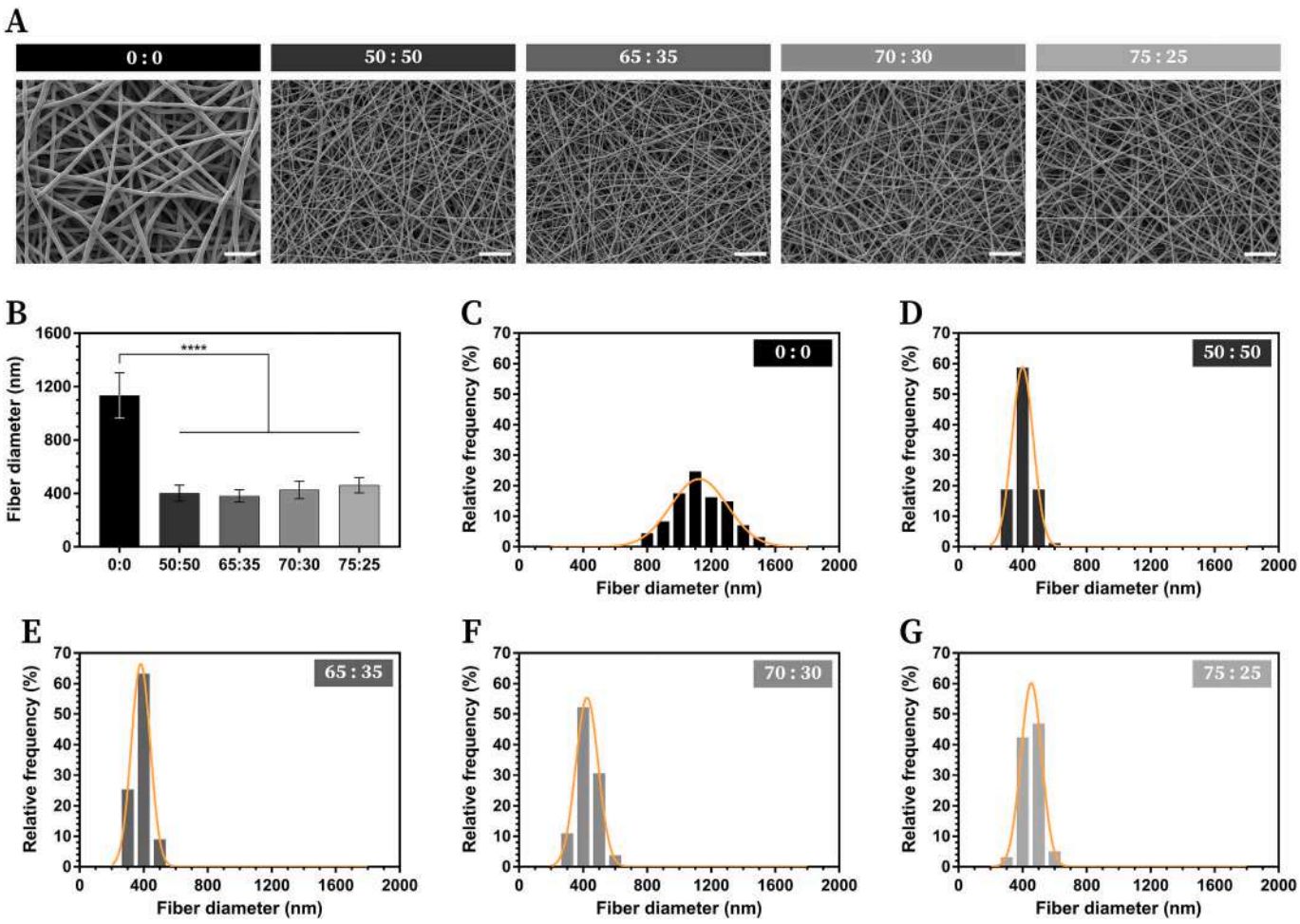

Fig. 4. ES of PEOT/PBT/(CN/PEG) composites. (A) SEM micrographs highlighting the nanofiber morphology obtained with the chosen compositions. Scale bar: 10 μm. (B) Bar graph summarizing the average fiber diameter for each condition ($n = 150$). Statistical analysis was performed using one-way ANOVA followed by a Tukey's HSD post-hoc test. (C–G) Frequency distribution analysis of the corresponding fiber diameters, demonstrating a narrower Gaussian curve (orange) for electrospun scaffolds with CN.

nanocomposites was evaluated by performing tensile tests on the produced films. Compression molded PEOT/PBT films displayed a maximum elongation of over 850 % before break, while composites 65:35, 70:30 and 75:25 had elongations of 100 %, 178 % and 78 % respectively (Fig. S6A). The rise in PEG content to a ratio of 50:50, which resulted in a homogeneous distribution of the pre-composite in films, demonstrated a relatively higher fracture strain of 230 %. In terms of the mechanical behavior in the elastic region, no significant differences were detected among the tested conditions (Fig. S6B). An average *E* value ranging between 68 and 80 MPa was obtained for all the films, without any noticeable trend dependent on the material composition.

Subsequently, the mechanical relevance of PEOT/PBT/(CN/PEG) nanocomposites for creating functional TM replacements was investigated using their biofabricated scaffolds. For this, tensile and indentation measurements were performed to evaluate the structural reinforcement offered by CN to the electrospun meshes. Fig. 6A(i) demonstrates the experimental setup applied for conducting the uniaxial tensile tests on nanofibrous scaffolds fabricated with the chosen CN/PEG compositions. In general, a stronger mechanical response was obtained for the PEOT/PBT/(CN/PEG) nanocomposites; however, it was not possible to precisely correlate the efficiency of the PEG-guided CN dispersion with their resultant stress-strain curves (Fig. 6A(ii)). Furthermore, the *E* computed within the linear elastic regime, demonstrated a notable increase upon inclusion of CN in the electrospun meshes (Fig. 6A(iii)). Although despite the increasing trend of *E* with the reduction of PEG, no statistically significant differences were observed between the selected CN/PEG ratios, analogous to their respective stress-strain curves. Therefore, the subsequent indentation studies were conducted only for the 50:50 condition.

The macroindentation approach has been regarded as a relevant characterization technique for TM scaffolds. A previously reported *ad-hoc* experimental setup was implemented (Fig. 6B(i)) (Anand et al., 2021). Similar to the tensile measurements, an elevated mechanical response was noted for the PEOT/PBT/(CN/PEG) nanocomposite, which was also reflected in the corresponding *E* value (Fig. 6B(ii)). An *E* of 11.27 ± 1.22 MPa was calculated for the composite membranes in comparison to 7.01 ± 0.69 MPa for the pristine ones (Fig. 6B(iii)). Therefore, these results highlighted the ability of CN in reinforcing electrospun scaffolds for TM repair.

3.6. Biodegradation characterization

The rate and extent of degradation was investigated to verify the durability of the electrospun TM scaffolds. A previously reported experimental setup was implemented for this, which has been illustrated schematically in Fig. 7A. After 6 months, the nanocomposite samples demonstrated a weight loss by 6.9 % ± 0.6 %, which was slightly higher than the 4.1 % ± 1.3 % noted in case of pristine PEOT/PBT scaffolds (Fig. 7B). A similar trend was observed at the end of one year, where a final biodegradation of 8.4 % ± 0.1 % was recorded for the electrospun

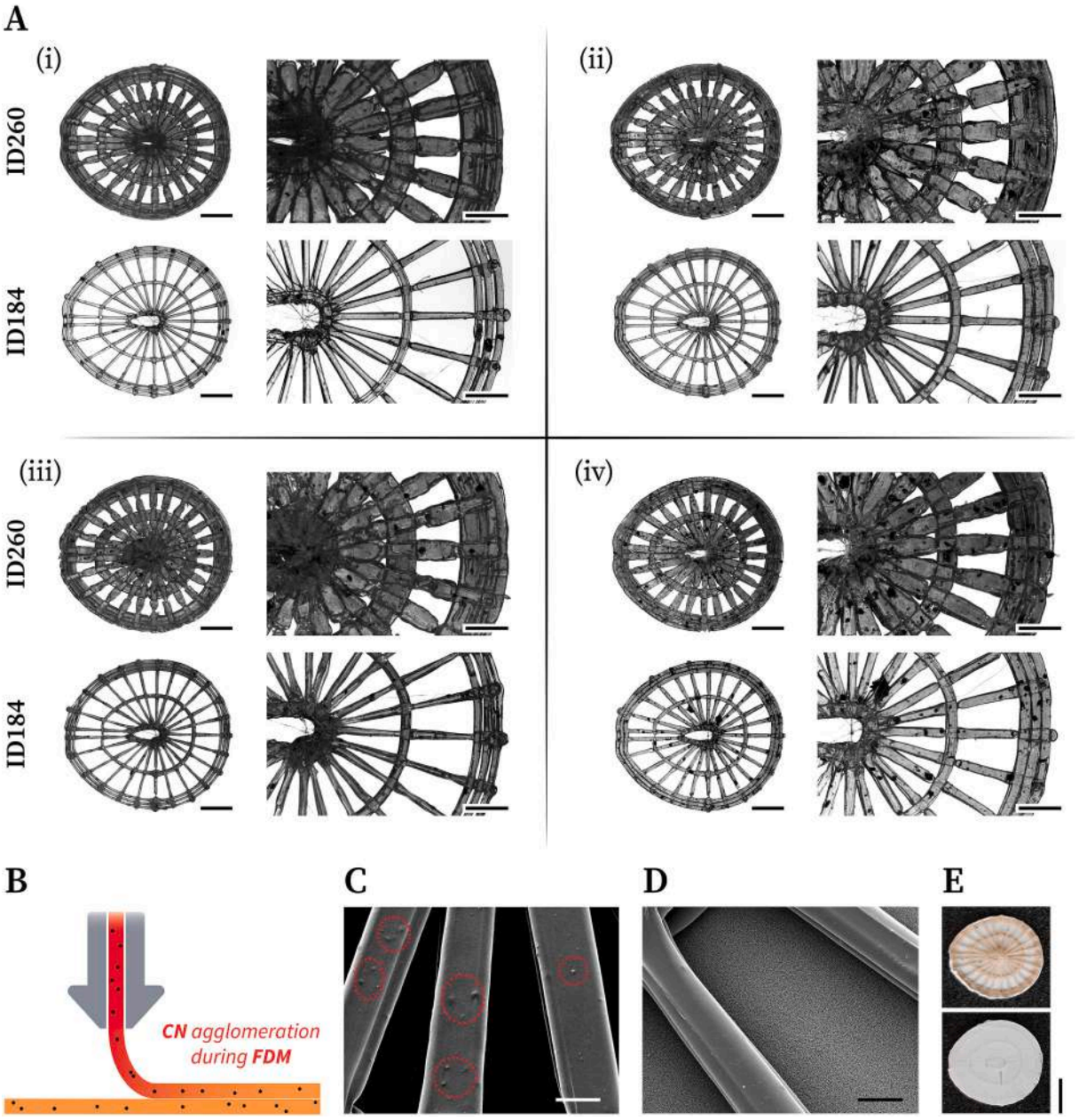

Fig. 5. FDM of PEOT/PBT/(CN/PEG) composites. (A) Stereomicroscope images of the fabricated TM scaffolds at lower (scale bar: 2 mm) and higher (scale bar: 1 mm) magnifications: (i) 50:50; (ii) 65:35; (iii) 70:30; and (iv) 75:25. (B) Schematic representation of CN agglomeration during the printing process. (C) SEM micrographs confirming the presence of CN aggregates (red dashed-lined circles) within the FDM filaments (scale bar: 200 μm). (D–E) Successful fabrication of dual-scale TM scaffolds with 50:50 PEOT/PBT/(CN/PEG) nanocomposite – (D) as observed under SEM (scale bar: 200 μm); and (E) pictures of front view: top, and back view: bottom (scale bar: 4 mm). (For interpretation of the references to colour in this figure legend, the reader is referred to the web version of this article.)

Table 1
Average filament diameters obtained for additive manufactured TM constructs using different nozzles and nanocomposites.

Needle	0:0	50:50	65:35	70:30	75:25
ID260	521 μm	483 μm	493 μm	501 μm	507 μm
ID184	216 μm	177 μm	191 μm	180 μm	221 μm
ID100	113 μm	–	–	–	–
ID70	102 μm	–	–	–	–

meshes with CN and 4.9 % ± 1.5 % for the ones without. In conclusion, the presence of CN was found to accelerate the scaffold disintegration process, resulting in statistically significant differences between the cumulative weight losses computed for the two polymers at the end of every month (M1–M12).

The obtained rate of degradation was slow in both the cases, which is desirable to allow the necessary cell migration and infiltration for the subsequent extracellular matrix (ECM) deposition. Moreover, the SEM analysis performed on the degraded samples at the end of this study, revealed an identical nanofibrous morphology with respect to the initial electrospun scaffolds highlighted in Fig. 4A. This was confirmed using high and low magnification micrographs of the sample surface and cross-section (Fig. 7C). Finally, no sign of bulk degradation was detected in the form of pores or cavities, which suggested the occurrence of surface erosion, characterized by a gradual superficial degradation of the electrospun fibers.

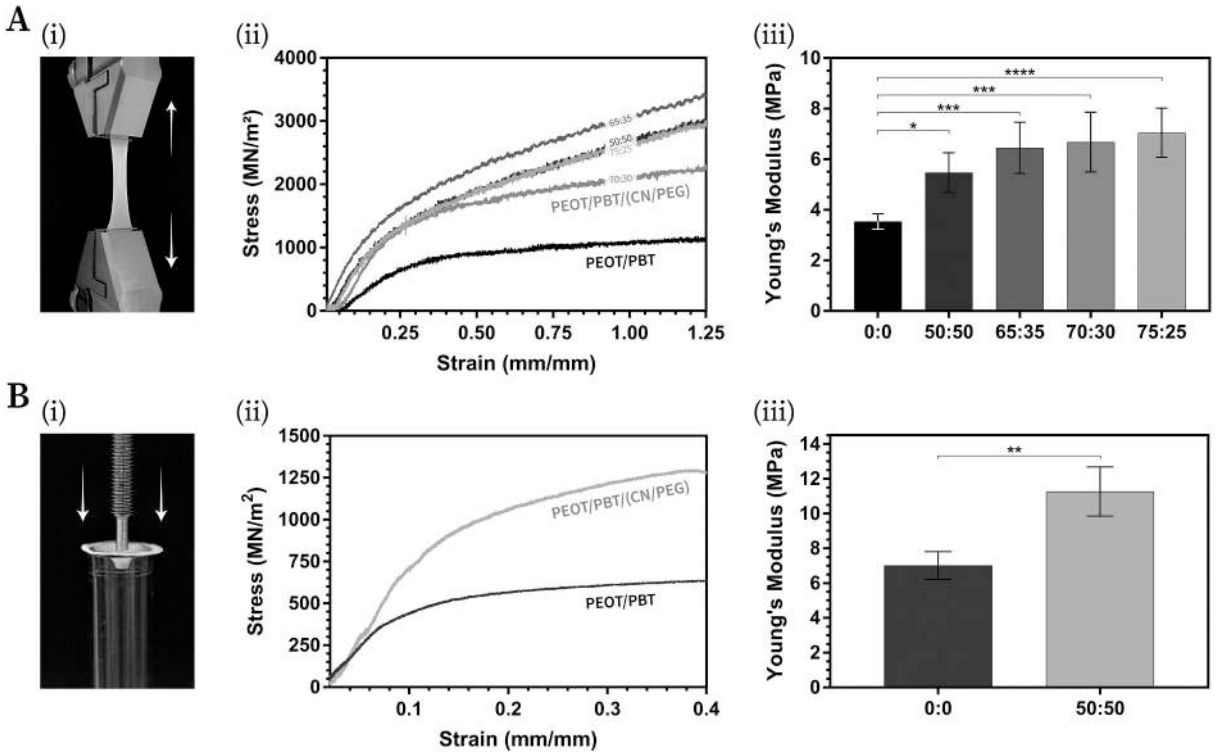

Fig. 6. Mechanical characterization of TM scaffolds. (A) Tensile measurements ($n = 5$): (i) pictorial representation of the setup implemented; (ii) stress-strain curves attained with the chosen compositions; (iii) average Young's moduli computed within the linear elastic regime. (B) Indentation measurements ($n = 4$): (i) pictorial representation of the setup implemented; (ii) stress-strain curves obtained for pristine PEOT/PBT (0:0) and PEOT/PBT/(CN/PEG) (50:50); (iii) average Young's moduli calculated for the two conditions. Statistical analyses were performed using one-way ANOVA followed by a Tukey's HSD post-hoc test.

3.7. Biological characterization

In vitro assessment of PEOT/PBT/(CN/PEG) nanocomposites was performed with respect to oto- and cytocompatibility of the fabricated films and electrospun scaffolds. In this regard, OC-k3 cells, which are inner ear epithelial cells, were applied for evaluating their direct and indirect compatibility with the delicate inner ear environment. CellTiter 96® AQueous Non-Radioactive Cell Proliferation assay was conducted to assess their viability when directly in contact, and when indirectly exposed to the culture medium conditioned with different composite films (Fig. 8A–B). The direct contact test, which was performed under the cell adhesion modality, showed a slight reduction in the OC-k3 viability in contrast to the control (Fig. 8A). Whereas on the other hand, the indirect test highlighted an excellent viability, comparable to that of the non-treated condition (Fig. 8B). Thus, these results confirmed that there are no ototoxicity constraints on the use of CN due to any possible diffusion of leachable compounds to the inner ear cells.

Furthermore, in addition to the OC-k3 cells, hMSCs were employed considering their growing prominence in TM tissue engineering. AlamarBlue® test was performed on the cultured cells to assess the cytocompatibility of the compression molded PEOT/PBT film and compression molded PEOT/PBT/(CN/PEG) films with different ratios of CN/PEG (Fig. 8C). The results revealed that, on day 1, the metabolic activity of hMSCs seeded on pristine PEOT/PBT films was higher than that detected on the different nanocomposites, with the compression molded PEOT/PBT being the highest one. However, after 3 days in culture, all the samples demonstrated a comparable value, where no statistically significant differences were noted among the chosen PEOT/PBT/(CN/PEG) formulations.

Finally, the 50:50 composition was selected to investigate the corresponding cellular behavior on electrospun scaffolds. A remarkable increase in the metabolic activity was detected for hMSCs cultured on the electrospun scaffold in comparison to the initial film (Fig. 8D). The nanofibrous surface topography of electrospun meshes allowed a superior cell attachment and proliferation, resulting in an average metabolic activity of 153 %, which was more than twice of that obtained for films on day 8. To further corroborate the quantitative findings, qualitative assessment was conducted in the form of SEM analysis. The micrographs revealed that, in general, the hMSCs adhered on both films and electrospun scaffolds, although they did that at a higher density in case of the latter (Fig. 8E). The nanofibrous morphology of the 50:50 nanocomposite facilitated a homogeneous growth and proliferation of hMSCs during 8 days of culture.

4. Discussion

Regenerative therapies for the eardrum have gained an increasing attention in the recent years. With the ongoing advancements in biomaterials and biofabrication techniques, several tissue engineering approaches have been proposed for treating the perforated TMs (Hussain & Pei, 2021). In the past, biomimetic scaffolds with appropriate geometry and material properties have been reported with a focus on reconstructing the entire eardrum (Anand et al., 2021; Kozin et al., 2016; Mota et al., 2015). Full TM constructs have been regarded crucial for repairing total and subtotal perforations; however, the current clinical needs indicate a comparatively higher prevalence of medium-size central perforations, which instead demand a partial reconstruction strategy (Olowookere et al., 2008). Therefore, the primary goal of this work was to investigate the application of carbohydrate-based composite materials for TM regeneration, with a special attention towards the widespread medium-size perforations.

A polysaccharide-derived crystalline nanomaterial, CN, was chosen for this, in combination with PEOT/PBT, a well explored copolymer for biofabricating TM scaffolds. The CN have evolved as a promising nanofiller for tissue engineering, owing to their excellent biocompatibility, immunomodulation and antimicrobial response (Ji et al., 2012).

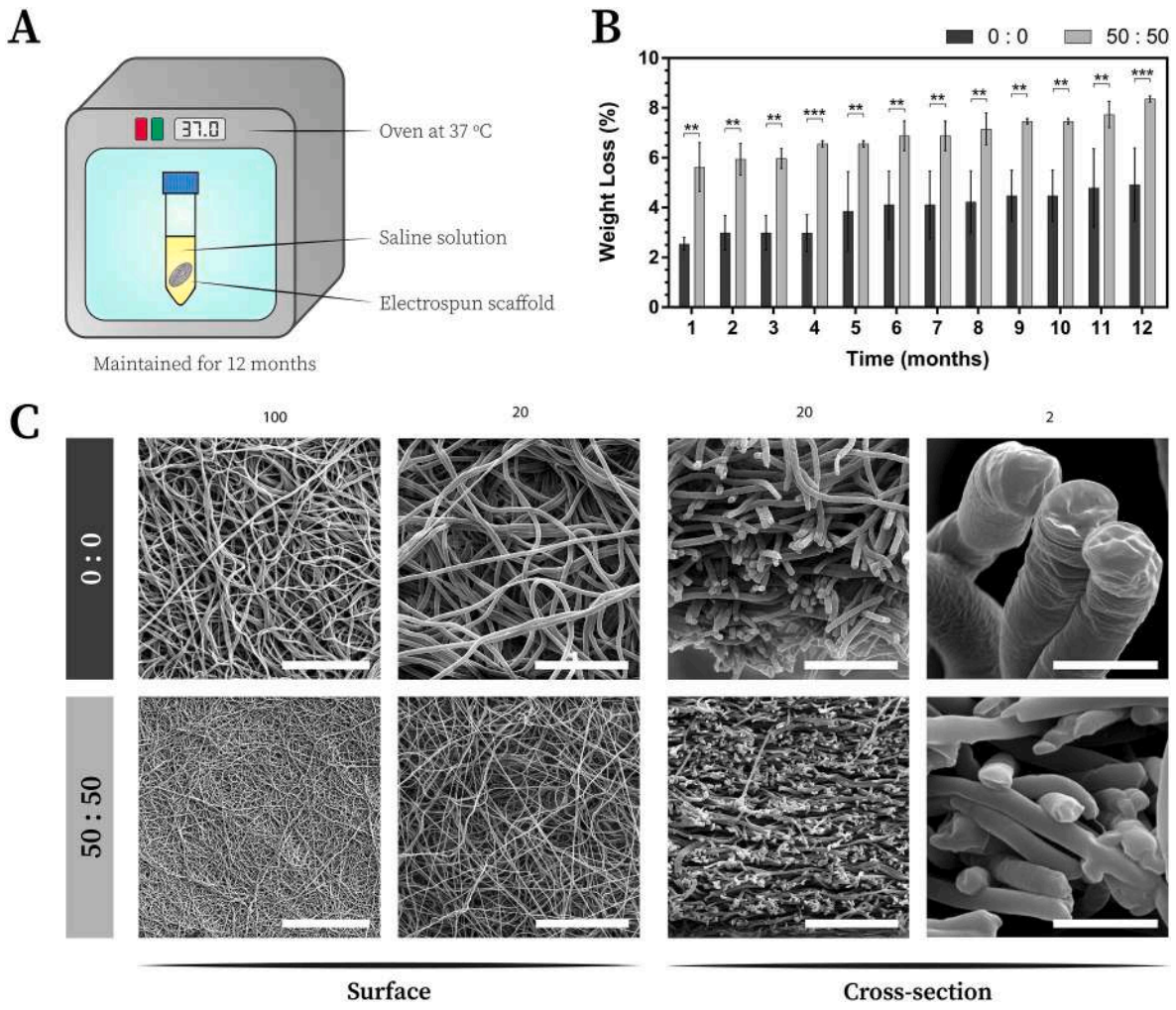

Fig. 7. Biodegradation test of TM scaffolds. (A) Schematic representation of the performed degradation study; (B) Bar graph showing weight loss of pristine PEOT/PBT (0:0) and PEOT/PBT/(CN/PEG) (50:50) electrospun meshes at different time intervals ($n = 3$). (C) SEM micrographs of the studied electrospun scaffolds after 12 months. Scale bar: 100 μm, 20 μm, 20 μm, and 2 μm (from left to right). Statistical analysis was performed using one-way ANOVA followed by a Student's *t*-test, considering $*p < 0.05$.

A longitudinal and transverse modulus of 150 GPa and 15 GPa, respectively, have been reported for the chitin nanocrystal, which advocates the utilization of nanosized chitins to introduce appreciable mechanical reinforcements within polymeric scaffolds (Zeng et al., 2012). In this regard, a preliminary characterization of the chosen grade of CN was conducted before investigating it as novel material for TM regeneration. The cyto- and otocompatibility assessment of the pristine CN demonstrated a favorable influence on the cultured cells; thus, validating its relevance for the application aimed herein.

One of the key objectives for an optimal nanocomposite production is to limit the spontaneous aggregation of the CN. The high surface energy of CN is known to promote these agglomerate formations, which subsequently hinders the uniform distribution within the polymer matrix (Malafeev et al., 2020). In this regard, PEG has been proposed as a favorable dispersion agent, capable of reducing hydrogen bonding interactions of the CN while further enhancing the wettability of the consequent nanocomposites (Li et al., 2017). Moreover, the presence of PEG blocks during the polymerization process of PEOT/PBT, is anticipated to stimulate a superior interfacial compatibility between the CN/PEG pre-composite and the polymer matrix. Therefore, in this study, the role of PEG was investigated for successful production of the PEOT/PBT/(CN/PEG) composites possessing favorable characteristics for TM reconstruction. Four compositions with different CN/PEG ratios (50:50, 65:35, 70:30, 75:25) were chosen to identify the most effective CN dispersion achieved with the minimal PEG concentration. In general, a low PEG content is preferable to reduce its influence on the physicochemical and biological properties of PEOT/PBT.

The effect of the different CN/PEG ratios was investigated within the formulated nanocomposites and their corresponding films. Being a relatively simpler approach in comparison to the latest biofabrication techniques, the polymeric films allowed a prompt and reproducible inspection of the selected compositions in terms of their physicochemical and morphological behavior. The XRD and FTIR spectra of PEOT/PBT/(CN/PEG), before and after compounding the pristine PEOT/PBT with CN/PEG, confirmed the inclusion of CN within the final nanocomposites. Moreover, they demonstrated that using high temperatures of 165 °C and 170 °C during the compounding and film production, respectively, did not alter the chemical structure of their constituents. Additionally, SEM analysis of the PEOT/PBT/(CN/PEG) films was performed to gain an initial understanding of PEG's impact over the process of melt compounding. Qualitative micrographic assessment of the corresponding longitudinal and transverse surfaces indicated an increased roughness with decreasing PEG content. This observation could be attributed to the viscosity mismatch generated during the blending procedure (Nerkar et al., 2014), where a higher PEG concentration allows a greater consistency between the pre-composite and PEOT/PBT with respect to their relative viscosities.

Following the preliminary characterization of the bulk

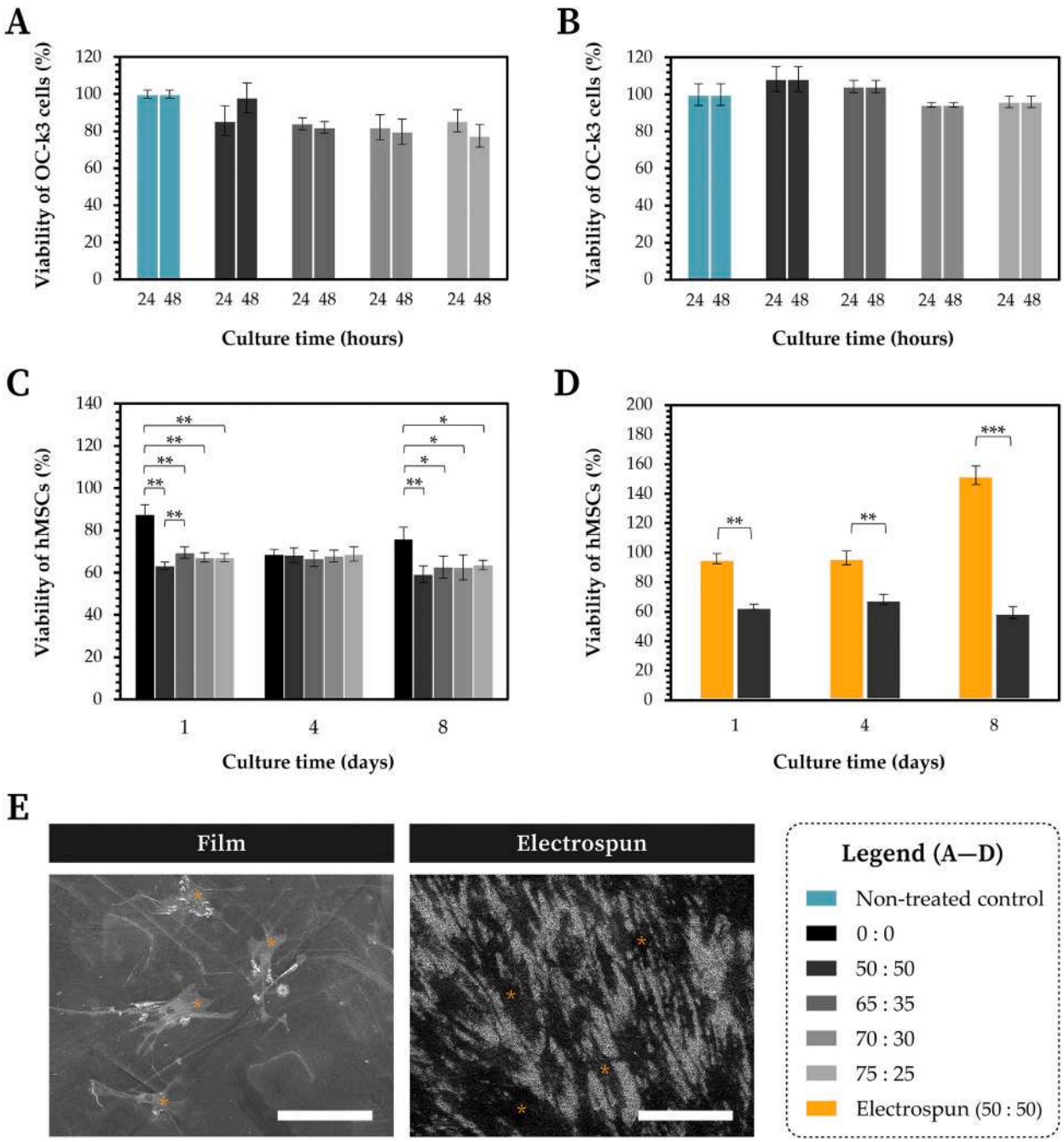

Fig. 8. *In vitro* assessment of PEOT/PBT/(CN/PEG) nanocomposites. The oto- and cyto-compatibility evaluation of the fabricated films and electrospun scaffolds ($n = 3$). (A, B) CellTiter 96® AQueous Non-Radioactive Cell Proliferation assay results, showing viability percent of OC-k3 cells, (A) in contact with the films (direct test), (B) or exposed to film-conditioned culture medium (indirect test). Cell viability is expressed in percentage as mean value ± standard deviation, where non-treated OC-k3 cells at 24 h and 48 h are considered 100 %. (C, D) AlamarBlue® assay results showing metabolic activity of the hMSCs cultured for 8 days (direct test) on: (C) all the investigated films, and (D) electrospun scaffold of the 50:50 composition, compared against its film counterpart. (E) SEM micrographs of hMSCs cultured on the surface of the 50:50 nanocomposite: film and electrospun scaffold. Cells have been marked by * as an example to distinguish them from the substrate surface. Scale bar: 200 μm.

nanocomposites, they were assessed in terms of their processability for fabricating biomimetic replacements for the perforated eardrum. The techniques of ES and FDM were tested considering their relevance for constructing PEOT/PBT based TM scaffolds (Anand et al., 2021; Danti et al., 2015; Mota et al., 2015). A hierarchical combination of the two approaches was envisaged for the full TM reconstruction, where a previously reported *in silico* model was employed to design and validate a suitable 3D architecture. The mechano-acoustical simulations performed on the reconstructed TM demonstrated a comparable response to the native tissue. In case of partial reconstruction, ES alone was investigated as the appropriate biofabrication strategy. The electrospun nanofibrous membranes have been considered an effective grafting substitute for medium-size TM perforations (Danti et al., 2015; Lee et al., 2014; Moscato et al., 2020; Seonwoo et al., 2019), although they often lack the desirable acousto-mechanical properties (Anand et al., 2021). Therefore, this study examines the introduction of carbohydrate-derived reinforcement agents that could fill the existing gap in material properties and allow the creation of functional patches for the eardrum.

Among the two biofabrication techniques, ES was applied first. A three-fold reduction in the electrospun fiber diameters was observed upon the addition of CN, resulting in a closer replication of the extracellular collagen fibrils (Wess, 2005). The DLS measurements suggest that the observed drop in fiber diameters could be credited to an increase in electroactivity of the precursor ES solutions. Inherently, the CN are known to carry a positive surface charge due to the protonation of its amine groups (NH_3^+) upon solubilization in acidic solvents such as hydrochloric acid, tetrafluoroethylene, and chloroform (Ji et al., 2012; Mincea et al., 2012; Morganti et al., 2018). With the collector being grounded, inclusion of electropositive charges induced additional stretching of the ES jet in whipping region, thereby leading to smaller nanofibers in nanocomposite meshes as compared to pristine PEOT/PBT (Haider et al., 2018). Moreover, this was also accompanied with narrowing of the Gaussian distribution curve, which indicated the role of CN in enhancing the homogeneity of electrospun membranes. The presented results highlighted these clear distinctions in the fiber dimensions obtained for PEOT/PBT/(CN/PEG) composites and pristine PEOT/PBT; however, no statistically significant differences were noted between the chosen CN/PEG ratios. Besides, the two blending approaches (melt and solution), applied for incorporating the CN within the PEOT/PBT matrix, were found to be comparable in terms of the respective electrospun membranes obtained.

Along with ES, melt extrusion or FDM based additive manufacturing has been widely explored to manipulate PEOT/PBT copolymer for diverse tissue engineering applications (Cámara-Torres, Duarte, et al., 2021; Cámara-Torres, Sinha, et al., 2021; Sinha et al., 2021). The current study attempted to further expand the relevance of this biofabrication technique with regard to the processability of polysaccharide-loaded PEOT/PBT composites. In general, the CN was effectively incorporated within the fabricated TM scaffolds, which was confirmed by the presence of brown spots throughout the deposited filament. The observed spots were hypothesized to be aggregates of CN, clustered together at high temperature. Considering the onset temperature of degradation for CN has been reported to be around 260 °C (Riehle et al., 2019), an accelerated agglomeration was seen at the printing temperature of 190 °C. Moreover, the extrusion of these CN aggregates was not an issue for the large needles, such as ID260 and ID184, but they led to recurrent clogging in the case of ID100 and ID70. This phenomenon restricted the creation of full TM scaffolds within the anatomical dimensions (thickness < 100 μm) of the native tissue. Nevertheless, hierarchical scaffolds were manufactured as a proof-of-concept to demonstrate that an integration of FDM with ES is still possible for PEOT/PBT/(CN/PEG) composites, although not for TM regeneration.

ES alone was selected as the primary biofabrication strategy with a strong emphasis towards the treatment of medium-size TM perforations. This work aimed to highlight the applicability of CN to produce mechanically reinforced electrospun patches for a partial reconstruction of the damaged tissue. In the past, silk fibroin was shown to be successful in reinforcing PCL based electrospun meshes for TM regeneration (Lee et al., 2014). The ability to control the material properties is a critical requirement for the creation of tissue engineered eardrum constructs. Earlier efforts in this direction for PEOT/PBT have revealed the possibility to enhance the acousto-mechanical response by manipulating the scaffold geometry (Anand et al., 2021). However, in case of a partial reconstruction, adapting the geometrical design is not trivial. Therefore, this study focused on achieving it by incorporating a carbohydrate-derived nanofiller that could simultaneously promote immunomodulatory and antimicrobial activity as well (Danti et al., 2021).

Considering the notable advantages of CN when compounded with thermoplastics (Coltelli et al., 2019; Ji et al., 2012; Kuo & Ku, 2008), they were chosen as the suitable reinforcing agent for PEOT/PBT. An E value of 4.38 MPa has recently been reported for PEOT/PBT based electrospun TM scaffolds, which was almost four-fold lower than the average E calculated for the native tissue (16.09 MPa) (Aernouts et al., 2012; Anand et al., 2021; Daphalapurkar et al., 2009; Huang et al., 2008; Von Békésy & Wever, 1960). The current work showed that this drawback could be significantly minimized by the introduction of CN within the polymer matrix. Tensile and indentation measurements were performed to confirm a similar trend in the observed mechanical response. In addition, tensile tests were used to compare a range of PEG formulations for their efficacy in dispersing CN within the electrospun meshes, although definitive conclusions could not be drawn. Therefore, the 50:50 CN/PEG ratio was chosen for the TM-specific indentation measurements. An E value of 11.27 MPa was computed for the PEOT/PBT/(CN/PEG) scaffolds in contrast to 7.01 MPa for the pristine ones. Future work in this regard will focus on the use of higher CN concentrations to attain E values resembling that of the native eardrum.

A timely biodegradation of the employed materials has been one of the fundamental challenges of tissue engineering. The rate and extent of degradation often governs the long-term efficacy of biofabricated scaffolds in achieving the desired tissue regeneration (Lee et al., 2012). In general, a predictable rate allows a simultaneous deposition of ECM by the host cells as the implanted polymer gradually disintegrates. Therefore, to further corroborate the clinical relevance of the electrospun patches proposed in this study, an *in vitro* biodegradation test was performed for 12 months. The obtained results demonstrated a controlled weight loss, accompanied by an excellent retention of the nanofibrous morphology, thereby suggesting a gradual surface degradation of both PEOT/PBT and PEOT/PBT/(CN/PEG) scaffolds. The slower rate of degradation is particularly desirable for treating pathological derived TM perforations, such as CSOM, which are comparatively more difficult to repair than the traumatic ones (Hussain & Pei, 2021). The ongoing inflammation and infection in case of the microbial-induced injuries usually leads to a reduced self-healing capability of the eardrum. In this regard, a steady rate of degradation is crucial to provide the required mechanical stabilization for a longer duration and facilitate a more homogenous regeneration of the perforated TM (Uebersax et al., 2006).

As highlighted earlier, the TM is known to exhibit an inherent regenerative ability, which allows the spontaneous healing of most acute perforations (Reijnen & Kuijpers, 1971). However, in case of large perforations, a tangible support in the form of bioactive patches is essential to assist the epithelium migration by latent progenitor cells (Kim et al., 2015). This cellular infiltration and subsequent regeneration of the connective tissue layer is necessary to reach an optimal acoustic performance after healing. Therefore, the biological response of the fabricated TM scaffolds holds a significant role in repopulating the damaged tissue and restoring its functionality. In the past, hMSCs have been investigated as a suitable candidate to reconstruct the *pars tensa*, which is a connective tissue layer comprising radially and circumferentially aligned collagen fibers produced by TM fibroblasts (Anand et al., 2021; Danti et al., 2015; Moscato et al., 2020; Mota et al., 2015). For this reason, hMSCs were chosen as the relevant cell type to assess the cytocompatibility of the PEOT/PBT/(CN/PEG) nanocomposites. Preliminary assessment on the fabricated films demonstrated favorable results for all the CN/PEG ratios unanimously. Moreover, when investigated on electrospun scaffolds, the 50:50 CN/PEG formulation of PEOT/PBT/(CN/PEG) revealed a significantly higher metabolic activity of hMSCs in comparison to its film counterpart. This finding is in line with other studies reported on the influence of surface morphology in steering cell-matrix interactions with respect to cell adhesion and proliferation (Denchai et al., 2018).

Finally, the TM replacement even though placed in the middle ear compartment, could potentially leach out molecules that might migrate to the cochlea and affect the inner ear environment. The inner ear is an intricate part of the human ear, where sensory cells transform the mechanical stimuli into electrical signals (Whitfield, 2015). Therefore, in addition to hMSCs, OC-k3 cells, HaCaT and PC-12 were applied to identify any potential ototoxicity due to putative nanocomposite leachable compounds towards the delicate inner ear epithelium (Astolfi et al., 2015). Both direct and indirect cytocompatibility tests performed on the CN and nanocomposite films confirmed a high viability of the

cultured OC-k3, HaCaT and PC-12 cells. In comparison, the direct cytocompatibility test required an adequate adhesion of the cells on the nanocomposite surface, which was not the case for indirect cytocompatibility test, where the cultured cells were exposed to nanocomposite films eluting in the culture media. This could explain the slight reduction in cellular activity detected for the direct tests as opposed to their indirect counterparts. Furthermore, in contrast to the untreated controls, the 50:50 CN/PEG composition showed relatively higher viability of OC-k3 cells during the indirect cytotoxic assessment, thereby indicating than any small molecular weight molecule potentially capable of crossing the middle ear compartment towards the cochlea, should not be harmful to the sensory cells. In summary, the developed PEOT/PBT/(CN/PEG) nanocomposites are cytocompatible with relevant cell types of the ear, and specifically the 50:50 CN/PEG formulation in the form of electrospun scaffolds appear as a fitting candidate for TM repair.

5. Conclusions

This work focused on the application of CN for improving the current regenerative therapies to treat TM perforations. It highlighted that the mechanical properties required for an optimal eardrum restoration can be achieved by reinforcing the PEOT/PBT copolymeric matrix using carbohydrate-derived nanofillers. Such modifications can be valuable for the fabrication of biomimetic patches to repair medium-size perforations of the TM, that cannot heal spontaneously. These injuries currently constitute the majority of the myringoplasty surgeries, and therefore, present an unmet clinical need. The homogeneous distribution of CN within the PEOT/PBT matrix is essential for the creation of consistent and reproducible nanocomposites. PEG was employed as an appropriate dispersion agent, where different CN/PEG ratios were investigated to ensure a uniform dispersion of CN. SEM micrographs of the bulk nanocomposites revealed a superior surface morphology in case of the highest PEG concentration chosen in this study. The ES and FDM tests conducted with the PEOT/PBT/(CN/PEG) composites validated their use for biofabrication driven tissue engineering, but the printing resolution of FDM limited their integration for the total TM reconstruction. A three-fold reduction in the diameter of electrospun nanofibers was noted with the inclusion of CN. Furthermore, as envisaged, an enhancement in mechanical properties, demonstrated by both tensile and macroindentation measurements, was accomplished with the prepared nanocomposites. Finally, the biological studies confirmed the cytocompatibility of the CN-based composites with excellent cell adhesion and proliferation, especially in case of the electrospun meshes. Future efforts in this direction will focus on the role of CN in promoting desired cell migration and intracellular collagen production to corroborate their relevance for an efficient TM regeneration.

CRediT authorship contribution statement

Shivesh Anand: Investigation, Validation, Formal analysis, Writing – Original draft preparation. **Bahareh Azimi**: Investigation, Validation. **Mónica Lucena**: Investigation, Validation, Formal analysis. **Claudio Ricci**: Investigation. **Mariarita Candito**: Investigation. **Lorenzo Zavagna**: Investigation, Formal Analysis. **Laura Astolfi**: Methodology, Validation, Supervision. **Maria-Beatrice Coltelli**: Methodology. **Andrea Lazzeri**: Resources, Methodology. **Stefano Berrettini**: Resources, Visualization. **Lorenzo Moroni**: Resources, Funding acquisition, Supervision, Writing - Reviewing and editing. **Serena Danti**: Conceptualization, Funding acquisition, Supervision, Writing - Reviewing and editing. **Carlos Mota**: Conceptualization, Resources, Funding acquisition, Supervision, Writing - Reviewing and editing.

Declaration of competing interest

The authors declare that they have no known competing financial interests or personal relationships that could have appeared to influence the work reported in this paper.

Data availability

Data will be made available on request.

Acknowledgments

Funding: This study was funded by the 4NanoEARDRM project, under the frame of EuroNanoMed III, an ERA-NET Cofund scheme of the Horizon 2020 Research and Innovation Framework Programme of the European Commission, the Netherlands Organisation for Scientific Research (NWO, grant number OND1365231), and the Italian Ministry of Education, University and Research (MIUR, grant number B56H18000140001). The Centre for Instrumentation Sharing, University of Pisa, is acknowledged for SEM analysis. Dr. Delfo D'Alessandro (University of Pisa) is kindly acknowledged for his technical support to SEM analysis.

Appendix A. Supplementary data

Supplementary data to this article can be found online at https://doi.org/10.1016/j.carbpol.2023.120732.

References

Aernouts, J., Aerts, J. R., & Dirckx, J. J. (2012). Mechanical properties of human tympanic membrane in the quasi-static regime from in situ point indentation measurements. *Hearing Research, 290*(1–2), 45–54.

Anand, S., Danti, S., Moroni, L., & Mota, C. (2022). Regenerative therapies for tympanic membrane. *Progress in Materials Science, 127*, Article 100942.

Anand, S., Stoppe, T., Lucena, M., Rademakers, T., Neudert, M., Danti, S., & Mota, C. (2021). Mimicking the human tympanic membrane: The significance of scaffold geometry. *Advanced Healthcare Materials, 10*(11), Article 2002082.

Askari, F., Zandi, M., Shokrolahi, P., Tabatabaei, M. H., & Hajirasoliha, E. (2019). Reduction in protein absorption on ophthalmic lenses by PEGDA bulk modification of silicone acrylate-based formulation. *Progress in Biomaterials, 8*, 169–183.

Astolfi, L., Simoni, E., & Martini, A. (2015). OC-k3 cells, an in vitro model for cochlear implant biocompatibility. *Hearing, Balance and Communication, 13*(4), 166–174.

Bertolaso, L., Martini, A., Bindini, D., Lanzoni, I., Parmeggiani, A., Vitali, C., & Previati, M. (2001). Apoptosis in the OC-k3 immortalized cell line treated with different agents: Apoptosis en linea celular OC k3 inmortalizada, tratada con diferentes agentes. *Audiology, 40*(6), 327–335.

Blanshard, J. D., Robson, A. K., Smith, I., & Maw, A. R. (1990). A long term view of myringoplasty in children. *The Journal of Laryngology and Otology, 104*(10), 758–762.

Brown, E. E., & Laborie, M.-P. G. (2007). Bioengineering bacterial cellulose/poly (ethylene oxide) nanocomposites. *Biomacromolecules, 8*(10), 3074–3081.

Brugnerotto, J., Lizardi, J., Goycoolea, F., Argüelles-Monal, W., Desbrieres, J., & Rinaudo, M. (2001). An infrared investigation in relation with chitin and chitosan characterization. *Polymer, 42*(8), 3569–3580.

C. Muzzarelli P. Morganti Preparation of chitin and derivatives thereof for cosmetic and therapeutic use 2013 Google Patents.

Cámara-Torres, M., Duarte, S., Sinha, R., Egizabal, A., Álvarez, N., Bastianini, M., & Bonetto, A. (2021). 3D additive manufactured composite scaffolds with antibiotic-loaded lamellar fillers for bone infection prevention and tissue regeneration. *Bioactive Materials, 6*(4), 1073–1082.

Cámara-Torres, M., Sinha, R., Scopece, P., Neubert, T., Lachmann, K., Patelli, A., & Moroni, L. (2021). Tuning cell behavior on 3D scaffolds fabricated by atmospheric plasma-assisted additive manufacturing. *ACS Applied Materials & Interfaces, 13*(3), 3631–3644.

Caminos, L., Garcia-Manrique, J., Lima-Rodriguez, A., & Gonzalez-Herrera, A. (2018). Analysis of the mechanical properties of the human tympanic membrane and its influence on the dynamic behaviour of the human hearing system. *Applied Bionics and Biomechanics, 2018*.

Chen, C., Li, D., Yano, H., & Abe, K. (2019). Insect cuticle-mimetic hydrogels with high mechanical properties achieved via the combination of chitin nanofiber and gelatin. *Journal of Agricultural and Food Chemistry, 67*(19), 5571–5578.

Cima, L., Vacanti, J., Vacanti, C., Ingber, D., Mooney, D., & Langer, R. (1991). *Tissue engineering by cell transplantation using degradable polymer substrates*.

Coltelli, M.-B., Cinelli, P., Gigante, V., Aliotta, L., Morganti, P., Panariello, L., & Lazzeri, A. (2019). Chitin nanofibrils in poly (lactic acid)(PLA) nanocomposites: Dispersion and thermo-mechanical properties. *International Journal of Molecular Sciences, 20*(3), 504.

Danti, S., Anand, S., Azimi, B., Milazzo, M., Fusco, A., Ricci, C., & Lazzeri, A. (2021). Chitin nanofibril application in tympanic membrane scaffolds to modulate inflammatory and immune response. *Pharmaceutics, 13*(9), 1440.

Danti, S., Mota, C., D'alessandro, D., Trombi, L., Ricci, C., Redmond, S. L., & Berrettini, S. (2015). Tissue engineering of the tympanic membrane using electrospun PEOT/PBT copolymer scaffolds: A morphological in vitro study. *Hearing, Balance and Communication, 13*(4), 133–147.

Daphalapurkar, N. P., Dai, C., Gan, R. Z., & Lu, H. (2009). Characterization of the linearly viscoelastic behavior of human tympanic membrane by nanoindentation. *Journal of the Mechanical Behavior of Biomedical Materials, 2*(1), 82–92.

Denchai, A., Tartarini, D., & Mele, E. (2018). Cellular response to surface morphology: Electrospinning and computational modeling. *Frontiers in Bioengineering and Biotechnology, 6*, 155.

Deschamps, A. A., Grijpma, D. W., & Feijen, J. (2001). Poly(ethylene oxide)/poly (butylene terephthalate) segmented block copolymers: The effect of copolymer composition on physical properties and degradation behavior. *Polymer, 42*(23), 9335–9345.

Dvorak, D. W., Abbas, G., Ali, T., Stevenson, S., & Welling, D. B. (1995). Repair of chronic tympanic membrane perforations with long-term epidermal growth factor. *Laryngoscope, 105*(12 Pt 1), 1300–1304.

Elieh-Ali-Komi, D., & Hamblin, M. R. (2016). Chitin and chitosan: Production and application of versatile biomedical nanomaterials. *International Journal of Advanced Research, 4*(3), 411.

Gan, R. Z. (2018). Biomechanical changes of tympanic membrane to blast waves. *Advances in Experimental Medicine and Biology, 1097*, 321–334.

Ghassemifar, R., Redmond, S., Zainuddin, & Chirila, T. V. (2010). Advancing towards a tissue-engineered tympanic membrane: Silk fibroin as a substratum for growing human eardrum keratinocytes. *Journal of Biomaterials Applications, 24*(7), 591–606.

Gonçalves de Pinho, A. R., Odila, I., Leferink, A., van Blitterswijk, C., Camarero-Espinosa, S., & Moroni, L. (2019). Hybrid polyester-hydrogel electrospun scaffolds for tissue engineering applications. *Frontiers in Bioengineering and Biotechnology, 7*, 231.

Grote, J. J., Bakker, D., Hesseling, S. C., & van Blitterswijk, C. A. (1991). New alloplastic tympanic membrane material. *The American Journal of Otology, 12*(5), 329–335.

Günday, C., Anand, S., Gencer, H. B., Munafò, S., Moroni, L., Fusco, A., & Danti, S. (2020). Ciprofloxacin-loaded polymeric nanoparticles incorporated electrospun fibers for drug delivery in tissue engineering applications. *Drug Delivery and Translational Research, 10*(3).

Haider, A., Haider, S., & Kang, I.-K. (2018). A comprehensive review summarizing the effect of electrospinning parameters and potential applications of nanofibers in biomedical and biotechnology. *Arabian Journal of Chemistry, 11*(8), 1165–1188.

Huang, G., Daphalapurkar, N. P., Gan, R. Z., & Lu, H. (2008). A method for measuring linearly viscoelastic properties of human tympanic membrane using nanoindentation. *Journal of Biomechanical Engineering, 130*(1), Article 014501.

Hussain, Z., & Pei, R. (2021). Necessities, opportunities, and challenges for tympanic membrane perforation scaffolding-based bioengineering. *Biomedical Materials, 16*(3), Article 032004.

Ji, Y. L., Wolfe, P. S., Rodriguez, I. A., & Bowlin, G. L. (2012). Preparation of chitin nanofibril/polycaprolactone nanocomposite from a nonaqueous medium suspension. *Carbohydrate Polymers, 87*(3), 2313–2319.

Kim, S. W., Kim, J., Seonwoo, H., Jang, K. J., Kim, Y. J., Lim, H. J., & Choung, Y. H. (2015). Latent progenitor cells as potential regulators for tympanic membrane regeneration. *Scientific Reports, 5*, 11542.

Kozin, E. D., Black, N. L., Cheng, J. T., Cotler, M. J., McKenna, M. J., Lee, D. J., & Remenschneider, A. K. (2016). Design, fabrication, and in vitro testing of novel three-dimensionally printed tympanic membrane grafts. *Hearing Research, 340*, 191–203.

Kuo, C. Y., Wilson, E., Fuson, A., Gandhi, N., Monfaredi, R., Jenkins, A., & Reilly, B. (2018). Repair of tympanic membrane perforations with customized bioprinted ear grafts using chinchilla models. *Tissue Engineering Part A, 24*(5–6), 527–535.

Kuo, Y. C., & Ku, I. N. (2008). Cartilage regeneration by novel polyethylene oxide/chitin/chitosan scaffolds. *Biomacromolecules, 9*(10), 2662–2669.

Lamme, E. N., Druecke, D., Pieper, J., May, P. S., Kaim, P., Jacobsen, F., & Steinstraesser, L. (2008). Long-term evaluation of porous PEGT/PBT implants for soft tissue augmentation. *Journal of Biomaterials Applications, 22*(4), 309–335.

Lee, H., Jang, C. H., & Kim, G. H. (2014). A polycaprolactone/silk-fibroin nanofibrous composite combined with human umbilical cord serum for subacute tympanic membrane perforation; an in vitro and in vivo study. *Journal of Materials Chemistry B, 2*(18), 2703–2713.

Lee, O. J., Lee, J. M., Kim, J. H., Kim, J., Kweon, H., Jo, Y. Y., & Park, C. H. (2012). Biodegradation behavior of silk fibroin membranes in repairing tympanic membrane perforations. *Journal of Biomedical Materials Research Part A, 100*(8), 2018–2026.

Levin, B., Redmond, S. L., Rajkhowa, R., Eikelboom, R. H., Atlas, M. D., & Marano, R. J. (2013). Utilising silk fibroin membranes as scaffolds for the growth of tympanic membrane keratinocytes, and application to myringoplasty surgery. *The Journal of Laryngology and Otology, 127*(Suppl. 1), S13–S20.

Li, J., Gao, Y., Zhao, J., Sun, J., & Li, D. (2017). Homogeneous dispersion of chitin nanofibers in polylactic acid with different pretreatment methods. *Cellulose, 24*(4), 1705–1715.

Lou, Z. C., & He, J. G. (2011). A randomised controlled trial comparing spontaneous healing, gelfoam patching and edge-approximation plus gelfoam patching in traumatic tympanic membrane perforation with inverted or everted edges. *Clinical Otolaryngology, 36*(3), 221–226.

Maharajan, N., Cho, G. W., & Jang, C. H. (2020). Application of mesenchymal stem cell for tympanic membrane regeneration by tissue engineering approach. *International Journal of Pediatric Otorhinolaryngology, 133*, Article 109969.

Malafeev, K., Moskalyuk, O., Yudin, V., Morganti, P., Ivan'kova, E., Popova, E. Vaganov, G., … (2020). Study of physicomechanical properties of composite fibers based on polylactide and modified chitin nanofibrils. *Polymer Science, Series A, 62*(3), 249–259.

Malheiro, A., Harichandan, A., Bernardi, J., Seijas-Gamardo, A., Konings, G. F., Volders, P. G., & Moroni, L. (2021). 3D culture platform of human iPSCs-derived nociceptors for peripheral nerve modelling and tissue innervation. *Biofabrication, 14*(1), Article 014105.

Mincea, M., Negrulescu, A., & Ostafe, V. (2012). Preparation, modification, and applications of chitin nanowhiskers: A review. *Reviews on Advanced Materials Science, 30*, 225–242.

Morganti, P., Danti, S., & Coltelli, M. B. (2018). Chitin and lignin to produce biocompatible tissues. *Research in Clinical Dermatology, 1*(01), 5–11.

Moscato, S., Rocca, A., D'Alessandro, D., Puppi, D., Gramigna, V., Milazzo, M., & Danti, S. (2020). Tympanic membrane collagen expression by dynamically cultured human mesenchymal stromal cell/star-branched poly(ε-caprolactone) nonwoven constructs. *Applied Sciences, 10*(9), 3043.

Mota, C., Danti, S., D'Alessandro, D., Trombi, L., Ricci, C., Puppi, D., & Berrettini, S. (2015). Multiscale fabrication of biomimetic scaffolds for tympanic membrane tissue engineering. *Biofabrication, 7*(2), Article 025005.

Nerkar, M., Ramsay, J. A., Ramsay, B. A., & Kontopoulou, M. (2014). Melt compounded blends of short and medium chain-length poly-3-hydroxyalkanoates. *Journal of Polymers and the Environment, 22*(2), 236–243.

Olowookere, S., Ibekwe, T., & Adeosun, A. (2008). Patterns of tympanic membrane perforation in Ibadan: A retrospective study. *Annals of Ibadan postgraduate medicine, 6*(2), 31–33.

Reijnen, C. J., & Kuijpers, W. (1971). The healing pattern of the drum membrane. *Acta Oto-Laryngologica. Supplementum, 287*, 1–74.

Riehle, F., Hoenders, D., Guo, J., Eckert, A., Ifuku, S., & Walther, A. (2019). Sustainable chitin nanofibrils provide outstanding flame-retardant nanopapers. *Biomacromolecules, 20*(2), 1098–1108.

Schilder, A. G., Chonmaitree, T., Cripps, A. W., Rosenfeld, R. M., Casselbrant, M. L., Haggard, M. P., & Venekamp, R. P. (2016). Otitis media. *Nature Reviews Disease Primers, 2*(1), 1–18.

Seonwoo, H., Shin, B., Jang, K. J., Lee, M., Choo, O. S., Park, S. B., & Jang, J. H. (2019). Epidermal growth factor-releasing radially aligned electrospun nanofibrous patches for the regeneration of chronic tympanic membrane perforations. *Advanced Healthcare Materials, 8*(2), Article 1801160.

Shankar, S., Reddy, J. P., Rhim, J. W., & Kim, H. Y. (2015). Preparation, characterization, and antimicrobial activity of chitin nanofibrils reinforced carrageenan nanocomposite films. *Carbohydrate Polymers, 117*, 468–475.

Sinha, R., Cámara-Torres, M., Scopece, P., Falzacappa, E. V., Patelli, A., Moroni, L., & Mota, C. (2021). A hybrid additive manufacturing platform to create bulk and surface composition gradients on scaffolds for tissue regeneration. *Nature Communications, 12*(1), 1–14.

Uebersax, L., Hagenmüller, H., Hofmann, S., Gruenblatt, E., Müller, R., Vunjaknovakovic, G., & Meinel, L. (2006). Effect of scaffold design on bone morphology in vitro. *Tissue Engineering, 12*(12), 3417–3429.

Verhoeff, M., van der Veen, E. L., Rovers, M. M., Sanders, E. A., & Schilder, A. G. (2006). Chronic suppurative otitis media: A review. *International Journal of Pediatric Otorhinolaryngology, 70*(1), 1–12.

Volandri, G., Di Puccio, F., Forte, P., & Carmignani, C. (2011). Biomechanics of the tympanic membrane. *Journal of Biomechanics, 44*(7), 1219–1236.

Von Békésy, G., & Wever, E. G. (1960). *Experiments in hearing*. New York: McGraw-Hill.

Weber, D. E., Semaan, M. T., Wasman, J. K., Beane, R., Bonassar, L. J., & Megerian, C. A. (2006). Tissue-engineered calcium alginate patches in the repair of chronic chinchilla tympanic membrane perforations. *Laryngoscope, 116*(5), 700–704.

Wess, T. J. (2005). Collagen fibril form and function. *Advances in Protein Chemistry, 70*, 341–374.

Whitfield, T. T. (2015). Development of the inner ear. *Current Opinion in Genetics & Development, 32*, 112–118.

von Witzleben, M., Stoppe, T., Ahlfeld, T., Bernhardt, A., Polk, M. L., Bornitz, M., & Gelinsky, M. (2021). Biomimetic tympanic membrane replacement made by melt electrowriting. *Advanced Healthcare Materials, 10*(10), Article 2002089.

Zeng, J.-B., He, Y.-S., Li, S.-L., & Wang, Y.-Z. (2012). Chitin whiskers: An overview. *Biomacromolecules, 13*(1), 1–11.

Zonderland, J., Moldero, I. L., Anand, S., Mota, C., & Moroni, L. (2020). Dimensionality changes actin network through Lamin A/C and zyxin. *Biomaterials, 240*, Article 119854.